This article has been accepted for inclusion in a future issue of this journal. Content is final as presented, with the exception of pagination.

Electronically Reconfigurable Switch-Mode Contactless Microwave Sensor for Detecting Small Concentrations of Water in Milk

Nazmia Kurniawati, *Graduate Student Member, IEEE*, Paris Vélez, *Senior Member, IEEE*, Pau Casacuberta, *Member, IEEE*, Xavier Canalias, *Graduate Student Member, IEEE*, Gerard Sisó, and Ferran Martín, *Fellow, IEEE*

***Abstract*—The concept of reconfigurable switch-mode microwave sensing is introduced in this article for the first time and validated experimentally by means of a contactless liquid sensor devoted to detecting small concentrations of DI water in milk. The device is highly nonlinear and acts as a switch, i.e., the phase of the reflection coefficient (the output variable) exhibits a sudden variation when a certain predefined and controllable concentration of water in milk (the input variable) is attained. Such controllability in the threshold water concentration is electronically achieved by incorporating a varactor diode into the sensor. It consists of a microstrip transmission line terminated with a dumbbell defect-ground-structure (DB-DGS) resonator, the sensitive element, and the variable capacitance (varactor), plus the required electronics for diode polarization (biasing) and a small capillary used to drive the liquid under test (LUT) to the sensing region (the slot of the DB-DGS resonator). It is demonstrated that by tuning the voltage applied to the varactor diode, the threshold (switch) water concentration can be varied between 0.25% and 5%, thereby allowing determination of the product (milk) quality with different (controllable) purity margins. Moreover, the device can be used to assess the quality of different milks (fat, semi-skim, and skim). Two system versions are experimentally validated: one of them based on a vector network analyzer (VNA), and another one equipped with a gain-phase detector and the associated electronics necessary to retrieve and visualize the relevant information.**

***Index Terms*—Dumbbell defect-ground-structure (DB-DGS), liquid sensor, microstrip technology, microwave sensor, phase-variation sensor, switch-mode sensor, varactor diode.**

Received 2 September 2026; revised 15 September 2026; accepted 19 September 2026. This work was supported in part by the MCIN/AEI 10.13039/501100011033, Spain (ERDF European Union) under Project PID2022-139181OB-I00, Project PID2025-169278OB-I00, and Project CPP2021-009080; and in part by the AGAUR, Catalonia Government, under Project 2021SGR-00192 and Project 2024 ICREA 00114. The work of Paris Vélez was supported by the Ramón y Cajal Program under Project RYC2022-035819-I. The work of Xavier Canalias was supported by the Ministerio de Universidades, Spain, through Formación de Personal Investigador (FPI) Grant (Ayudas Para la Formación de Profesorado Universitario) under Grant PREP2022-000364. *(Corresponding author: Nazmia Kurniawati.)*

The authors are with CIMITEC, Departament d'Enginyeria Electrònica, Universitat Autònoma de Barcelona, 08193 Barcelona, Spain (e-mail: Nazmia.Kurniawati@uab.cat).

Digital Object Identifier 10.1109/TMTT.2026.3736781

I. Introduction

THE dairy industry (including milk and its byproducts) represents an important percentage of gross domestic product (GDP) in any developed country. For example, in Spain, it contributes to roughly 2% of the national GDP, but the percentage is higher in other countries of the EU and USA (with 3% of GDP as of 2023). In this context, the development of technology to aid in assessing and ensuring product (milk) quality during and after production is of vital importance. There are two aspects that might jeopardize product quality, i.e., adulteration (usually during postproduction stages) and product processing (involving cleaning of facilities, e.g., bottling plants, or sharing such facilities with other products, in both cases potentially generating contaminants, and thereby limiting product purity and hence quality).

Milk adulteration by adding water in small concentrations does not significantly alter its properties (taste, smell, and color), and hence subtle water adulteration might be unnoticed by consumers. Nevertheless, besides water, there are many other adulterants of milk, like emulsifying agents, caustic soda, urea, detergent, low-quality oils, and starch, which are employed to prepare synthetic milk, harmful to health [1], [2]. Thus, milk adulteration has been identified as an important issue by the Health and Food Safety Authorities. On the other hand, milk bottling plants are usually cleaned by dragging, using water or detergent diluted in water. Therefore, before bottling, it should be ensured that milk purity is better than a certain predefined threshold (or, equivalently, that the concentration of water is below an acceptable value).

According to the previous paragraph, monitoring systems to detect the presence of small concentrations of water, or any other kind of adulterant, in milk are highly demanded. Current methods to detect adulterants in milk are mainly based on spectroscopic techniques, including nuclear magnetic resonance (NMR), infrared (IR) spectroscopy, Raman spectroscopy, ultraviolet-visible (UV-Vis) spectroscopy, mass spectrometry, laser-based techniques, dielectric spectroscopy, and X-ray spectroscopy; see the review papers [3], [4], [5]. Such techniques are efficient in most cases but are costly and do not provide real-time detection in some cases. Thus, microwave-based techniques, where permittivity changes caused by the adulterant constitute the

0018-9480 © 2026 IEEE. All rights reserved, including rights for text and data mining, and training of artificial intelligence and similar technologies. Personal use is permitted, but republication/redistribution requires IEEE permission.
See https://www.ieee.org/publications/rights/index.html for more information.

This article has been accepted for inclusion in a future issue of this journal. Content is final as presented, with the exception of pagination.

sensing approach, have been reported [6], [7], [8], [9], [10], [11].

In the works presented in [6], [7], [8], and [10] a dielectric probe kit was used for sensing. This is an efficient (non-planar) approach to determine the dielectric properties of liquids, but it is expensive and requires postprocessing. By contrast, in [9] and [11], low-cost planar sensors based on substrate integrated waveguide (SIW) and microstrip technology, respectively, were reported. The sensor in [9] is a cavity resonator, whereas the one reported in [11] is a closed-loop microstrip antenna. Both sensors [9], [11] utilize the resonance frequency and magnitude variation for sensing. These sensors have demonstrated their functionality for detecting the presence of undesired products in milk, including water, but their sensitivity and resolution are limited. Thus, detecting small traces of water or adulterants in milk with such sensors is not without difficulty. Moreover, frequency-variation sensors (one of the most widespread classes within microwave sensors [12], [13], [14], [15], [16], [17], [18], [19], [20], [21], [22], [23], [24], [25], [26], [27], [28], [29], [30], [31], [32], [33], [34], [35]) require frequency sweeping signals for sensing, thereby increasing the cost of the associated electronics when low-cost systems [without the use of vector network analyzers (VNAs)] are required.

In recent years, single-frequency sensors, based on either magnitude [36], [37], [38], [39] or phase variation [40], [41], [42], [43], [44], [45], [46], [47], [48], [49], [50], [51], [52], [53], [54], [55], [56], [57], [58], [59], [60], [61], [62], [63], [64], [65], [66], [67], [68], [69], [70], [71], [72], [73], [74], [75], [76], [77], [78], [79], [80], [81], [82], [83], [84], [85], have been reported. These sensors simply need a harmonic (single-tone) signal for sensing. Such a signal can be generated by means of a harmonic oscillator or by means of a low-cost voltage-controlled oscillator (VCO). Concerning the output signal, determined by the dielectric properties of the material under test (MUT), or analyte, it can be obtained by means of an envelope detector (magnitude-variation sensors) or through a phase detector (phase-variation sensors).

Nevertheless, besides the cost-effective and simple associated electronics of single-frequency sensors, those based on phase variation exhibit two additional advantages: 1) robustness against electromagnetic interference (EMI) and noise (as far as phase measurements are involved) and 2) an unprecedented high sensitivity. Concerning this latter aspect, sensitivity is directly related to the slope of the phase response at the operating frequency, as discussed in [77]. Several techniques to boost up the phase slope (and hence the sensitivity) have been proposed, including the use of long meandered sensing lines [42], [44], artificial transmission lines [40], [43], [45], [46], [48], cascaded high/low impedance quarter-wavelength transmission line sections (acting as impedance inverters) terminated with a sensing resonator [47], [50], [51], [52], [53], [54], [57], [62], [66], [68], [75], [80], weakly coupled resonators [58], [59], [65], [76], [81], and structures exhibiting closely spaced resonance and antiresonance frequencies [73], [78], [82], [83], [84], [85]. In addition, it has been demonstrated that, in reflective-mode phase-variation sensors, losses tend to improve the sensitivity [63], [64], [72], [79].

A highly sensitive proximity sensor based on a loss-assisted (and tunable) sensitivity enhancement mechanism using a junction field-effect transistor (JFET) has been recently reported [72]. This sensor exhibits a peak sensitivity of 2291°/mm. On the other hand, a reflective-mode phase-variation sensor based on a pair of coupled dumbbell defect-ground-structure (DB-DGS) resonators, also assisted by losses, was able to detect the presence of less than 0.1% of isopropanol in deionized (DI) water, with a maximum sensitivity of 293°/%, and was also reported [76]. Finally, let us mention that a peak sensitivity of 6350° per unit of dielectric constant in a permittivity sensor based on a mechanically reconfigurable reflective-mode structure implemented by means of a complementary split-ring resonator (CSRR) terminating a transmission line has been reported [83] (this sensor exploits resonance/antiresonance). These performance indicators point out the potential of single-frequency reflective-mode phase-variation sensors.

In this work, the target is to detect small concentrations of DI water in milk using a low-cost planar sensor. Since the dielectric properties of water and milk are similar (as compared to those of alcohol, e.g., isopropanol and water, which are substantially different), an extremely high sensitivity (even assisted by losses) might not suffice for our purposes. Thus, we will design the device based on a novel concept, switch-mode operation, where the objective is to generate a sudden phase change (easily measurable) when a certain (predefined and controllable) concentration of water (threshold) is reached. Since different levels of milk purity (determined by the threshold water concentration) might be required, depending on the desired milk quality, such threshold concentration should be controllable. Consequently, the reported device incorporates a varactor diode to electronically tune the threshold concentration of water. Reconfigurable sensors based on varactor diodes have been proposed [85], [86], but, to the best of the authors' knowledge, a reconfigurable switch-mode operation microwave sensor like the one presented in this article has never been reported so far. This novel detection/sensing concept and its experimental validation by applying it to a case example of interest in the dairy industry (detection of small traces of water in milk) are the main contributions of the present article. In [84], a similar sensor devoted to detecting water in wine was proposed. The sensitivity and resolution of that sensor are very good, but such a device is not reconfigurable, which is the main relevant aspect of the sensor reported in this article. As will be seen, this aspect will be instrumental in controlling the threshold water concentration defining the level of the required product purity, regardless of the type of milk (fat, skim, or semi-skim).

The paper organization is as follows. Section II introduces the novel switch-mode sensing/detection concept, which will be applied to detect small concentrations of water in milk. Emphasis is placed on the specific mechanism to achieve such a highly nonlinear (switch-type) sensor response. Moreover, it is shown that, by using a varactor diode, it is possible to control the threshold water concentration. Experimental validation

This article has been accepted for inclusion in a future issue of this journal. Content is final as presented, with the exception of pagination.

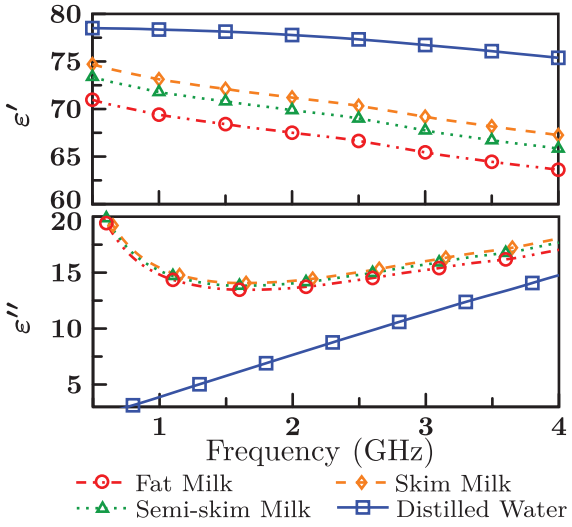


Fig. 1. Real (ε') and imaginary (ε'') parts of the complex dielectric constant of DI water and milk (fat, semi-skim, and skim) in the range 0.5–4.0 GHz, measured at T = 24 °C, as inferred with the *DAKS-35 R140B* dielectric probe. The milk characterized is *Leche Hacendado*, distributed by Spanish company *Mercadona*.

of this switch-mode operation, including electronic control of the threshold value (reconfigurability), is the subject of Section III. This section demonstrates the possibility of detecting water concentration above various thresholds (achieved by tuning the bias voltage applied to the varactor) for fat, skim, and semi-skim milks. The possibility of using a gain-phase detector, avoiding the use of a VNA, is the main subject of Section IV. A comparative analysis is carried out in Section V. Finally, Section VI concludes the work.

II. Proposed Switch-Mode Sensing Concept and Analysis

In a recent paper by authors [87], a planar reflective-mode phase-variation sensor was designed and applied to determine the water concentration in milk. The sensor response for small water concentrations was quasi-linear, with an average sensitivity of roughly $S_{\text{av}} = -6°/\%$ and an (optimistic) resolution of 1% (a value that results from assuming that the system can discern phase changes of 6°). Such sensitivity is much smaller than the sensitivity achieved in other liquid sensors devoted to determining solute concentration in binary mixtures. For example, as indicated in the introduction, in the liquid sensor reported in [76], the maximum sensitivity was found to be 293°/%, with a resolution better than 0.1%. However: 1) this sensor operates in direct contact with the liquid under test (LUT) and, most important and 2) the complex permittivity values of DI water and isopropanol (the components used in the binary mixture in [76]) are very different. Both aspects were instrumental in achieving the indicated (excellent) sensitivity and resolution. By contrast, the sensor reported in [86] was contactless (a capillary was used to drive the LUT to the sensing region), and the dielectric properties of milk and water are similar, especially the real part of the permittivity, as depicted in Fig. 1 (this explains the worse sensor performance indicators, as compared to the device presented in [76]).

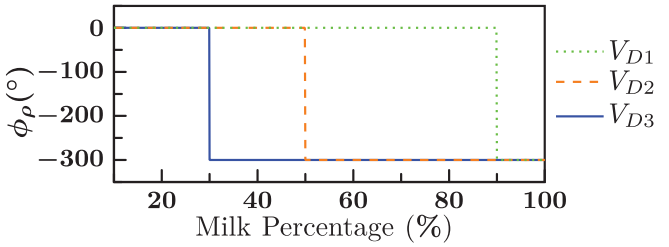


Fig. 2. Sketch of the (ideal) phase response of a reconfigurable switch-mode phase-variation sensor. The threshold levels (corresponding to the milk percentages where the phase suddenly changes), as well as the phase states (high and low) and voltages applied, are arbitrary.

A. Reconfigurable Switch-Mode Sensor Concept

The target in this article is to implement a sensor able to detect smaller concentrations of DI water in milk, as compared to [87], operating as a switch, namely, generating a sudden change in the phase response when a certain concentration of water (called the threshold) is achieved. Moreover, the sensor should be able to satisfy the following requirements.

1) Electronically tune the threshold water concentration, so that different margins of product (milk) purity can be defined.
2) Exhibit its functionality for different kinds of milk (fat, semi-skim, and skim).

If the phase response exhibits a sudden change at a predefined threshold water concentration, detecting when such water content in milk is reached is relatively easy. Thus, the intended system should operate, ideally, as a binary sensor, exhibiting two different states (phase levels) depending on whether the water concentration exceeds the threshold value or not. This switch-mode sensing concept, including the reconfigurability to tune the threshold level, is illustrated in Fig. 2. This highly nonlinear (switch-type) and tunable response is not possible with conventional approaches. For electronic tuning, a variable reactance or conductance is needed (in this article, a varactor diode will be used). To generate a switch-mode phase response, we will deliberately use the effect of losses and design the sensor such that a change of regime, from the high-loss to the low-loss regime, occurs for the desired threshold concentration of water, an aspect to be discussed next. Moreover, the sensor will be implemented as a one-port reflective-mode device, since the effect of losses on the phase response is more noticeable in such sensors, as compared to the transmission-mode counterparts, as discussed in [75].

B. Analysis on the Effects of Losses, Circuit Model, and Simulations

Let us assume that the considered one-port sensor can be described by a complex impedance given by

$$Z_{\text{in}}(\omega) = R(\omega) + j\chi(\omega) \tag{1}$$

where the real, $R(\omega)$, and the imaginary, $\chi(\omega)$, parts depend on the angular frequency, ω. By considering that the reference impedance of the ports is Z_0, the reflection coefficient is given by

$$\rho(\omega) = \frac{Z_{\text{in}}(\omega) - Z_0}{Z_{\text{in}}(\omega) + Z_0} = \frac{R(\omega) + j\chi(\omega) - Z_0}{R(\omega) + j\chi(\omega) + Z_0} \tag{2}$$

This article has been accepted for inclusion in a future issue of this journal. Content is final as presented, with the exception of pagination.

and the reflection coefficient at the resonance angular frequency, ω_0, where the reactance nulls [$\chi(\omega_0) = 0$], is

$$\rho(\omega_0) = \frac{R(\omega_0) - Z_0}{R(\omega_0) + Z_0}. \tag{3}$$

The phase of the reflection coefficient, the variable of interest, is

$$\phi_\rho(\omega) = \arctan\left\{\frac{\chi(\omega)}{R(\omega) - Z_0}\right\} - \arctan\left\{\frac{\chi(\omega)}{R(\omega) + Z_0}\right\} \tag{4}$$

and the phase slope at resonance is given by [77]

$$\left.\frac{d\phi_\rho(\omega)}{d\omega}\right|_{\omega_0} = \frac{2Z_0}{R^2(\omega_0) - Z_0^2}\left.\frac{d\chi(\omega)}{d\omega}\right|_{\omega_0}. \tag{5}$$

According to these expressions, it follows that if (ideally) losses are absent [$R(\omega) = 0$], the reflection coefficient at resonance is $\rho(\omega_0) = -1$, the corresponding phase is $\phi\rho(\omega_0) = \pm 180°$ (i.e., providing a phase jump in the wrapped phase response), and the phase slope is negative, see expression (5), since the derivative of the reactance [last term in (5)] in any lossless network should always be a positive number, according to the Foster's reactance theorem [88]. However, if losses cannot be neglected, the relative weight between $R(\omega_0)$ and Z_0 determines the phase response of the circuit. Namely, if $|R(\omega_0)| < Z_0$ (low-loss regime), the phase of the reflection coefficient at resonance is identical to that of the lossless case [$\phi\rho(\omega_0) = \pm 180°$], and the phase slope is negative. However, if $|R(\omega_0)| > Z_0$ (high-loss regime), the phase of the reflection coefficient at resonance is zero [$\phi\rho(\omega_0) = 0°$], and the phase slope is positive at that frequency. Finally, for the situation corresponding to critical coupling [$|R(\omega_0)| = Z_0$], see [89], the reflection coefficient at resonance is null and the phase slope is infinite. Under critical coupling, all the injected power is absorbed by the circuit at resonance (perfect matching).

An important aspect is that, in general, operation in either the low-loss or the high-loss regime does not depend only on device losses (conductive, dielectric, or radiation losses). It might also depend on the reactive elements of the circuit. Let us assume that the sensor under consideration can be described by a certain circuit model (at least in the vicinity of resonance), described by inductive, capacitive, and resistive elements. The above statement means that the magnitude of $R(\omega_0)$ can depend on the capacitances and inductances of the model [an exception is the series *RLC* resonator, where the real part of the impedance is simply $R(\omega_0) = R$]. Consequently, we cannot conclude that operation in the low-loss regime is guaranteed if losses are small. Indeed, in the proposed sensor, by merely changing a reactive element, it is possible to switch it from the low-loss to the high-loss regime, as it will be shown. However, obviously, such a change of regime can also be generated if the dielectric properties of a certain LUT (to be monitored by the sensor) change. This is the principle of the proposed switch-mode sensor, where, by merely tuning a capacitance (using a varactor diode), it is possible to control the water concentration that provides critical coupling and is identified as the threshold. The phase response below and above the threshold is radically different (because such threshold concentration delimits the change of regime), and for this reason, identification of such threshold concentration is conceptually simple (the sensor operates as a switch).

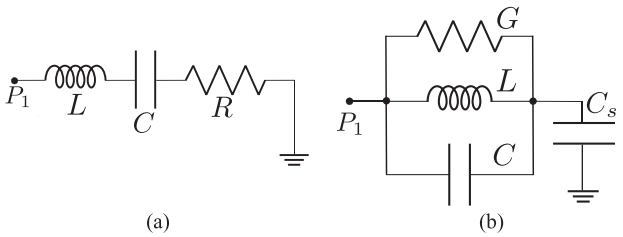


Fig. 3. (a) Circuit model of a one-port sensor based on a matched line terminated with an SIR and series resistor and (b) based on a matched line terminated with a DB-DGS resonator and a patch capacitor.

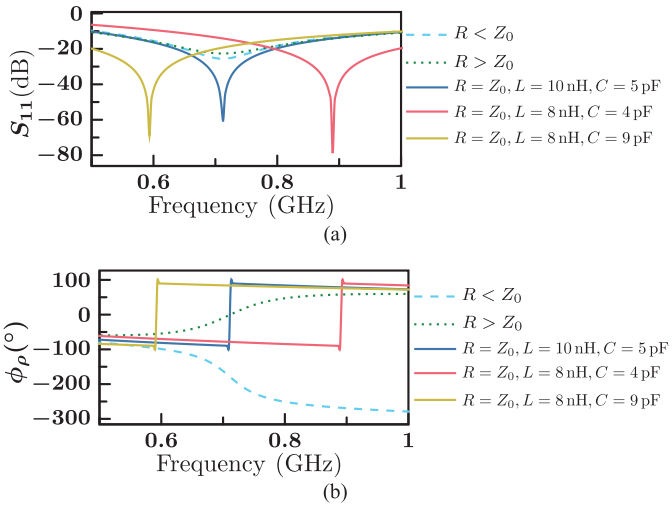


Fig. 4. (a) Magnitude and (b) phase responses of the circuit of Fig. 3(a) for $L = 10$ nH, $C = 5$ pF and $R = 45\ \Omega < Z_0 = 50\ \Omega$, $R = Z_0 = 50\ \Omega$ (critical coupling), and $R = 58\ \Omega > Z_0 = 50\ \Omega$. The figure also includes the responses for critical coupling. With $L = 8$ nH and different values of the capacitance, i.e., $C = 4$ pF and $C = 9$ pF. The phase is depicted unwrapped.

To gain insight into the effects of losses on the phase response, let us consider that two certain one-port sensing devices can be described by the circuits depicted in Fig. 3. In the circuit of Fig. 3(a), a series *RLC* resonator, the real and the imaginary parts of the impedance are given by

$$R(\omega) = R \tag{6}$$

and

$$\chi(\omega) = \omega L\left(1 - \frac{\omega_0^2}{\omega^2}\right) \tag{7}$$

respectively, where $\omega_0^2 = 1/LC$ is the squared angular resonance frequency. In this case, the operation regime is dictated only by R. Consequently, significant losses are needed to achieve critical coupling, or circuit operation in the high-loss regime. The magnitude and phase responses for three cases, $R < Z_0$, $R = Z_0$, and $R > Z_0$, with $Z_0 = 50\ \Omega$, are depicted in Fig. 4. For $R < Z_0$, the phase slope is negative at ω_0 and $\phi\rho(\omega_0) = -180°$ (the wrapped phase is depicted); for $R = Z_0$, the return loss is $RL = \infty$ at ω_0, whereas the phase exhibits an infinite slope at that frequency; finally, for $R > Z_0$, the phase slope is positive at ω_0 and $\phi\rho(\omega_0) = 0°$. For the circuit model of Fig. 3(a), a series-connected

This article has been accepted for inclusion in a future issue of this journal. Content is final as presented, with the exception of pagination.

resistance, with $R = Z_0$, is required to achieve critical coupling, and critical coupling will always occur (provided $R = Z_0$) regardless of the value of the reactive elements, L and C.

Let us assume that the dielectric properties of a certain analyte change and that such changes perturb the capacitance C (a reasonable assumption), but not the resistance R, and that $R = Z_0$. The phase and magnitude responses for different values of C are also depicted in Fig. 4. Due to the stepped phase responses under critical coupling, detecting when a certain capacitance value is attained (or, equivalently, when the analyte exhibits a certain value of the dielectric constant or related variable, e.g., a concentration in a binary solution) is easy. Such capacitance is merely given by the resonance frequency, in turn determined by the magnitude notch or by the phase singularity (jump). Nevertheless, a sensor described by the circuit model of Fig. 3(a), e.g., a matched feed line terminated by a step impedance resonator (SIR) [54], has an intrinsic limitation for liquid sensing based on a capillary, i.e., reduced sensitivity. In microstrip technology, the broadside capacitance of the SIR patch limits the sensitivity, unless the capillary is embedded in the substrate, a solution reported in [90], [91], and [92]. In coplanar waveguide (CPW) technology, the capillary should surround the perimeter of the SIR patch, where the field lines are significant, but this is not the best option in terms of robustness and isolation of the fluidic part.

For liquid sensing, either using fluidic channels and holders (contact-based sensors) or utilizing capillaries (contactless sensors), slot-type resonators are preferred. The circuit of Fig. 3(b) describes a microstrip transmission line terminated with a transversally etched DB-DGS resonator (modeled by the inductance L, the capacitance C, and the conductance G) and a capacitive patch (with capacitance C_s), as demonstrated in [84]. This is the sensor considered in this work, where a capillary aligned with the DB-DGS axis is added to drive the LUT close to the sensing element (the DB-DGS resonator). The introduction of the varactor diode for reconfigurability will be discussed later. For this circuit model [see Fig. 3(b)], even though the conductance G is small (such conductance includes device and LUT losses), the magnitude of the real part of the impedance at resonance can be comparable to or even higher than Z_0, since it depends on the reactive parameters according to

$$R(\omega_0) = \frac{G}{G^2 + \omega_0^2 C^2 \left(1 - \frac{\omega_p^2}{\omega_0^2}\right)^2} \tag{8}$$

where ω_p is the antiresonance (angular) frequency, given by

$$\omega_p = \frac{1}{\sqrt{LC}}. \tag{9}$$

The resonance angular frequency, ω_0, nulls the reactance, given by

$$\chi(\omega) = -\frac{1}{\omega C_s} - \frac{\omega C \left(1 - \frac{\omega_p^2}{\omega^2}\right)}{G^2 + \omega^2 C^2 \left(1 - \frac{\omega_p^2}{\omega^2}\right)^2}. \tag{10}$$

Thus, such frequency is

$$\omega_0^2 = \frac{2C^2\omega_p^2 + CC_s\omega_p^2 - G^2 - \sqrt{\left(G^2 - CC_s\omega_p^2\right)^2 - 4C^2G^2\omega_p^2}}{2C\left(C + C_s\right)} \tag{11}$$

a cumbersome expression that can be reduced to

$$\omega_0 = \frac{1}{\sqrt{L\left(C + C_s\right)}} \tag{12}$$

provided losses are sufficiently small. Approximation (12) is valid as far as $G^2 \ll 2C^2\omega_p^2$, $G^2 \ll CC_s\omega_p^2$, and $G^2 \ll C_s^2\omega_p^2/4$. Nevertheless, the most restrictive condition is the latter, since C_s should be small compared to C. The reason is that a small C_s/C ratio increases the phase slope between the resonance and antiresonance frequencies, since there is a significant variation of the phase between such frequencies, the ratio being given by

$$\frac{\omega_p}{\omega_0} = \sqrt{1 + \frac{C_s}{C}} \tag{13}$$

and the phase slope in such a frequency region must be high to use the sensor in switch mode.

Introducing (12) in (8) gives

$$R(\omega_0) = \frac{G}{G^2 + \omega_0^2 C_s^2}. \tag{14}$$

According to (14), the coupling between the source and the resonator [critical coupling ($|R(\omega_0)| = Z_0$), over-coupling ($|R(\omega_0)| > Z_0$), or under-coupling ($|R(\omega_0)| < Z_0$)] is determined by G and by the reactive elements. For a fixed value of the reactive parameters, let us calculate the value of G providing the maximum value of $R(\omega_0)$. For that purpose, we calculate the derivative of (14) with G, and force it to be null, i.e.,

$$\frac{dR(\omega_0)}{dG} = \frac{-G^2 + \omega_0^2 C_s^2}{\left(G^2 + \omega_0^2 C_s^2\right)^2} = 0. \tag{15}$$

Thus, the real part of the impedance at resonance, $R(\omega_0)$, is maximized for $G = \omega_0 C_s$, and the value of such impedance is

$$R(\omega_0)|_{G=\omega_0 C_s} = \frac{1}{2\omega_0 C_s}. \tag{16}$$

From (16), we can conclude that a necessary condition to achieve critical coupling is $2\omega_0 C_s < Y_0 = 1/Z_0$, equivalent to

$$\frac{2}{\sqrt{\frac{L}{C_s}\left(1 + \frac{C}{C_s}\right)}} < Y_0. \tag{17}$$

On the other hand, given a certain conductance G, the value of C_s providing critical coupling is found by forcing $R(\omega_0) = Z_0$. This gives

$$C_s = \frac{\left(\bar{G} - \bar{G}^2\right)Y_0^2 L + \sqrt{\left(\bar{G} - \bar{G}^2\right)^2 Y_0^4 L^2 + 4\left(\bar{G} - \bar{G}^2\right)Y_0^2 LC}}{2} \tag{18}$$

where $\bar{G} = G/Y_0$ is the normalized conductance. To obtain (18), we have introduced (12) in (14) and we have isolated C_s in the equation that results by equating (14) to Z_0. Inspection

This article has been accepted for inclusion in a future issue of this journal. Content is final as presented, with the exception of pagination.

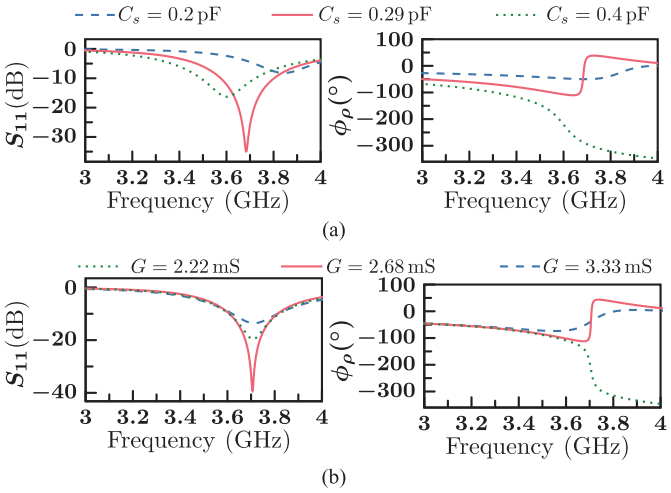


Fig. 5. Frequency responses (magnitude and phase of the reflection coefficient) for the circuit of Fig. 3(b) by varying (a) C_s and (b) G. The fixed reactive parameters are $L = 1.58$ nH and $C = 0.9$ pF. The phase is depicted unwrapped.

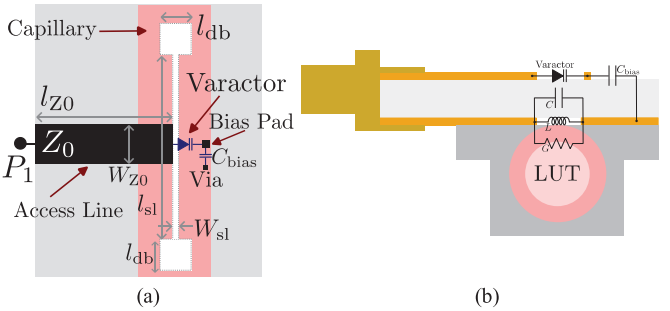


Fig. 6. (a) Layout and (b) cross-sectional view of the proposed sensor, not drawn to scale, including the varactor diode and the capillary. Dimensions (in mm) are: $W_{Z_0} = 3.36$, $l_{Z_0} = 30$, $l_{db} = 4$, $W_{sl} = 0.2$, and $l_{sl} = 40$. The access line is depicted in black, whereas the ground plane is depicted in gray. P_1 denotes the input port. Note that in the cross-sectional view, we have depicted the parallel resonant tank as caused by the DB-DGS resonator. However, in the circuit model, such a tank should be series-connected to the varactor diode, similar to the circuit of Fig. 3(b) (with such tank series-connected to the capacitance C_s).

of (18) reveals that a physical (positive) solution for C_s exists provided $\bar{G} - \bar{G}^2 > 0$, which means that the conductance should satisfy $G < Y_0$. Under this condition, critical coupling is achieved by adjusting the capacitance to the value given by (18), and such a value is compatible with (17).

If the reactive parameters satisfy (17), there are two mathematical solutions for G providing critical coupling, i.e.,

$$G = \frac{Y_0}{2}\left(1 \pm \sqrt{1 - 4Z_0^2\omega_0^2 C_s^2}\right). \tag{19}$$

These solutions have been inferred by isolating G from $R(\omega_0) = Z_0$, with $R(\omega_0)$ given by (14). However, it should be mentioned that, although the higher value of G (the one with the + sign) satisfies $G < Y_0$, such conductance does not actually provide critical coupling, because, to obtain (19), expression (14) has been used, and such expression is valid under the approximations indicated after (12), which assume that G must be very small. According to (19), as $C_s \to 0$, the conductance necessary to achieve critical coupling also tends to zero. Moreover, condition (17), or $2\omega_0 C_s < Y_0$, is also inferred from (19), since G must be a positive real number.

According to the previous discussion, C_s and G can be used to control the coupling (critical, over-coupling, or under-coupling) between the source and the circuit (sensor). This can be appreciated in Fig. 5, where the responses by varying C_s [see Fig. 5(a)] and by varying G [see Fig. 5(b)] in the vicinity of the critical coupling [$R(\omega_0) = Z_0 = 50\ \Omega$] are depicted. Such critical coupling can be generated with different combinations of C_s and G. In Fig. 5, the considered values of such elements (providing critical coupling) are $C_s = 0.29$ pF and $G = 2.68$ mS.

C. Proposed Sensor

In practice, considering the specific sensor implementation of this work (as shown in Fig. 6), where the sensing element is the DB-DGS resonator, G is determined by the properties of the analyte (milk with a certain water content, in our case), and by substrate and capillary losses. Thus, the conductance is not a control parameter unless a variable conductance is connected between both sides of the slot of the DB-DGS resonator. Nevertheless, this is not a good solution for tuning, since the capillary should be placed in contact with the slot and aligned with it. However, by terminating the matched access line with the DB-DGS resonator and with a varactor diode (rather than with a patch capacitance), as depicted in Fig. 6, tuning is possible, and the diode (acting as a variable capacitor), as well as the polarization circuitry, do not interfere with the capillary. Thus, tuning the bias voltage of the varactor diode has the effect of modifying the capacitance C_s, with the added advantage that such capacitance is merely controlled by the voltage applied to the diode, not by the electromagnetic properties of the analyte. Nevertheless, it should be mentioned that the diode is not a pure capacitor (it exhibits some losses and parasitic inductance), and hence the actual circuit model of the reconfigurable sensor is not as simple as that of Fig. 3(b). Section III shows the specific strategy to control the threshold water concentration by tuning the varactor diode and validates the approach.

III. Experimental Validation

The hypothesis to implement the switch-mode sensor able to detect small (controllable) concentrations of water in milk is to design the device such that when the capillary contains pure (100%) milk, it operates slightly over-coupled regardless of the diode capacitance (tuned by the bias voltage). In other words, the device should operate in the high-loss regime, but close to the onset of critical coupling. The reason is that adding a small quantity of DI water to milk has the effect of reducing losses, and hence G (see Fig. 1). Consequently, a switch to the low-loss regime is expected by adding a small quantity of water to milk. The presence of water also increases the capacitance of the DB-DGS resonator, C, since the real part of the complex permittivity of DI water is slightly higher than that of pure milk. Such an increase in C reduces the resonance frequency, see expression (14), and has the opposite effect than a reduction of G on $R(\omega_0)$. However, the relative variation of C by adding water to milk is expected to be small, as

This article has been accepted for inclusion in a future issue of this journal. Content is final as presented, with the exception of pagination.

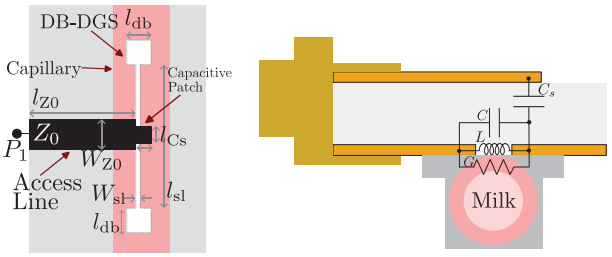


Fig. 7. (a) Layout and (b) cross-sectional view of the surrogate structure used for sensor design. Dimensions (in mm) are: $W_{Z_0} = 3.36$, $l_{Z_0} = 40$, $l_{db} = 4$, $W_{sl} = 0.2$, and $l_{Cs} = 2.6$. The access line is depicted in black, whereas the ground plane is depicted in gray. P_1 denotes the input port.

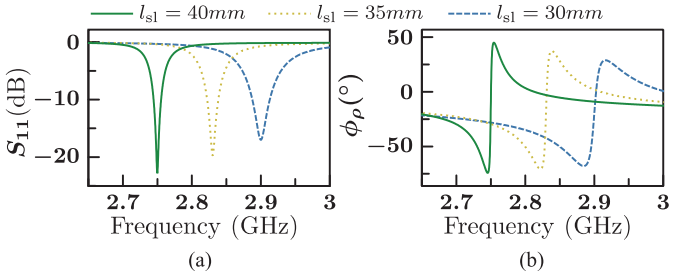


Fig. 8. Simulated frequency responses, i.e., (a) magnitude and (b) phase, of the surrogate structure for various lengths of the slot of the DB-DGS resonator. The electromagnetic simulations have been carried out with the *CST Microwave Studio* commercial software.

compared to the relative variation of G, since, according to Fig. 1, in the vicinity of 2.8 GHz (roughly the resonance frequency of the considered sensor with pure milk in the capillary), the dielectric constant of DI water and fat milk differs by approximately 18%, whereas the imaginary part of the permittivity differs by roughly 36%.

A. Sensor Design and Simulation

The design of the sensor has been carried out taking into account the following specifications and considerations: 1) resonance frequency set to roughly $f_0 = 2.8$ GHz when the capillary contains the REF sample (pure fat milk); 2) the capillary is made of Polyurethane, with internal and external diameters of 4.0 and 6.0 mm, respectively; 3) the substrate is the *Isola I-Tera MT40 (RF/MW)*, with thickness $h = 1.524$ mm, dielectric constant $\varepsilon_r = 3.55$, and loss tangent $\tan\delta = 0.0022$; and 4) the tunable element is the varactor diode model *SMV2019* from *Skyworks*, exhibiting a capacitance variation between 2.22 and 0.3 pF, for bias voltages tuned in the range 0–20 V. The choice of frequency obeys a tradeoff between DB-DGS dimensions (smaller as frequency increases) and sensor implementation without the use of a VNA, with the cost of associated electronics (phase detector, varactor, couplers, and isolators) increasing with frequency.

Emulating the operational conditions (with the presence of the varactor diode and the polarization circuit) in a simulation environment is not without difficulty. Thus, we have opted to proceed by considering a simplified (surrogate) structure for simulation purposes, where the diode is replaced by a square patch capacitance providing a value close to the minimum capacitance of the diode. The capillary full of fat milk is taken into account by considering the properties of both materials; see Fig. 7. As indicated before, the capacitance, C, of the DB-DGS resonator must be high, as compared to C_s. This means that an elongated DB-DGS resonator with the narrowest possible slot must be considered. Therefore, the inductance L of the resonator must be adjusted to the required (small) value to obtain the desired resonance frequency. This is achieved by properly tuning the dimensions of the square apertures of the DB-DGS resonator.

The specific design procedure is as follows. The access line is matched to the impedance of the port, i.e., $Z_0 = 50\ \Omega$, hence its width is the one indicated in the caption of Fig. 7, providing such characteristic impedance with the considered substrate. The length of this line (also indicated in the caption of Fig. 7) is not relevant since the access line merely introduces a phase shift that can be canceled. The dimensions of the patch capacitance terminating the line have been adjusted to obtain a capacitance of $C_s = 0.36$ pF. Finally, the side length of the square apertures of the DB-DGS resonator has been set to the value indicated in the caption of Fig. 7, and we have considered as a free parameter for tuning the length of the DB-DGS slot, l_{sl}. Fig. 8 depicts the responses for different DB-DGS slot lengths, where it is clearly shown that this length is instrumental in obtaining the desired resonance frequency, given by the notch in the magnitude response. As can be seen in Fig. 8, the device operates in the high-loss regime in all cases.

B. Sensor Fabrication

Using the dimensions of the surrogate structure as a starting point, we have fabricated the sensor, including the capillary and the varactor diode, and we have measured the frequency response with the capillary full of fat milk for different voltages applied to the diode bias circuit. Due to the parasitic elements of the diode (which justify in part the use of a surrogate model for sensor design), we have optimized the sensor from the measured responses, adjusting the length of the DB-DGS slot until the resulting resonance frequencies (for the different bias voltages applied to the varactor diode) lie in the vicinity of 2.8 GHz. Thus, it has been necessary to fabricate and measure various structures with different slot lengths, in order to find the optimum sensor (i.e., the one satisfying the previous specifications). The photograph of such a sensor, with $l_{sl} = 40$ mm, is shown in Fig. 9 (the device microwave module has been fabricated by means of the *LPKF ProtoMat S104* micro-milling machine). To provide mechanical stability, and thus ensure repeatability, the capillary has been securely fixed on top of the sensing element (the DB-DGS resonator) by using a polylactic acid (PLA) cover screwed to the substrate by means of Teflon screws (the 3-D-printer *FFF Ultimaker 3 Extended* has been used to fabricate the cover). Let us also indicate that in order to confine the electric field generated by the DB-DGS resonator within the analyte (milk), an aluminum tape has been sandwiched between the capillary and the cover, as depicted in Fig. 9.

An important aspect in fluidic sensors is to avoid air bubbles. To mitigate this aspect, the sensor and the capillary

This article has been accepted for inclusion in a future issue of this journal. Content is final as presented, with the exception of pagination.

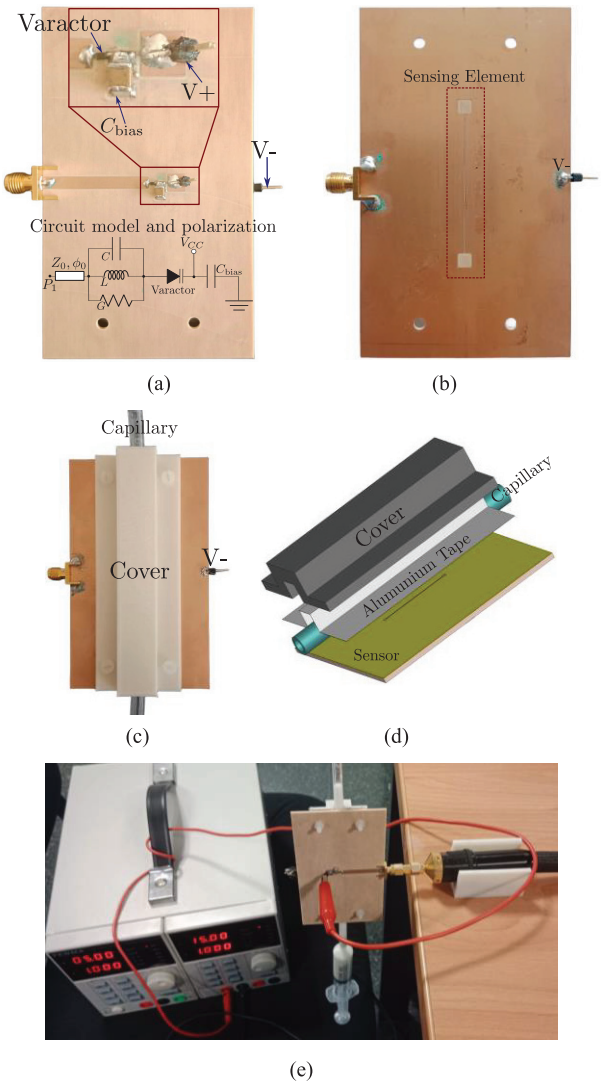


Fig. 9. Fabricated reconfigurable switch-mode sensor. (a) Photograph of the top view of the microwave module, including the varactor diode and necessary circuitry; (b) photograph of the bottom view of the microwave module (excluding the capillary); (c) photograph of the sensor including the capillary and the PLA cover; (d) exploded view (schematic) of the sensor; and (e) photograph of the sensor with polarization cables and measuring probes. Dimensions of the fabricated structure (in mm) are: $W_{Z_0} = 3.36$, $l_{Z_0} = 40$, $l_{db} = 4$, $W_{sl} = 0.2$, and $l_{sl} = 40$. The circuit model including diode biasing is depicted in (a).

are positioned vertically, and the LUT (milk with a certain concentration of water) is injected from the lower liquid port of the capillary; see Fig. 9(e). By these means, no air bubbles are present in the capillary. The temperature of the analyte has been controlled by means of a heater mantle (model *Labbox HMSD-500-001*) and a humidity chamber with controllable temperature (model *Memmert HCP50*). Thus, the temperature of the liquid has been set to $T = 24$ °C (the effects of varying the temperature are discussed in Section III-D).

C. Results and Validation

Fig. 10 depicts the measured frequency responses for the sensor of Fig. 9 with the capillary full of pure fat milk and different applied voltages (as the applied voltage, V_D, increases, the diode capacitance decreases). It can be seen

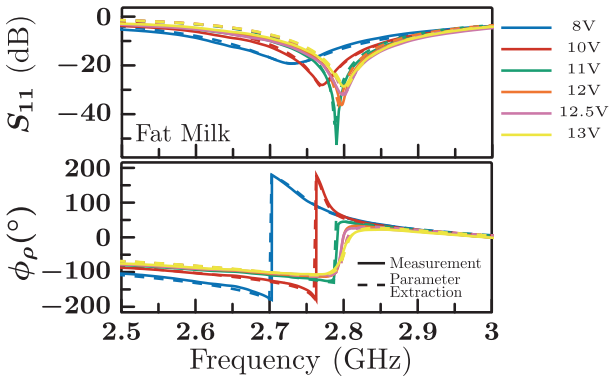


Fig. 10. Measured frequency responses, i.e., magnitude and wrapped phase, of the fabricated reconfigurable sensor for the indicated applied voltages, with the capillary containing 100% pure fat milk in all cases. The measurements have been carried out with the *Keysight 5221A* VNA. The circuit simulation with extracted parameters is included for comparison. The temperature is 24 °C.

TABLE I
PARAMETER EXTRACTION FOR THE RESPONSES OF FIG. 10

Loss Reg.	Bias (V)	C_s (pF)	L (nH)	C (pF)	G (mS)	$R(\omega_0)$ (Ω)
Low	8.0	0.67	1.49	1.77	4.01	28.73
Low	10.0	0.50	1.48	1.79	3.45	40.21
High	11.0	0.40	1.48	1.80	2.90	50.38
High	12.0	0.40	1.47	1.80	3.01	51.35
High	12.5	0.40	1.47	1.80	3.05	51.88
High	13.0	0.39	1.47	1.80	3.13	54.93

that for $V_D = 8$ and 10 V, the lower applied voltages (corresponding to the larger capacitances), the sensor is under-coupled (low-loss regime), exhibiting a negative phase slope at resonance (characterized by the $\pm 180°$ phase jump; the phase is depicted wrapped). However, for a slightly higher applied voltage ($V_D = 11$ V), the device switches to the over-coupled mode of operation (high-loss regime), and the phase slope at resonance is positive (and very high, since the sensor operates close to critical coupling). As the bias voltage increases (diode capacitance decreases), the sensor further enters the high-loss regime, and the phase slope (positive) at resonance decreases. Note that the resonance frequency increases with V_D, but such variation is very soft because the diode capacitance, C_s, is small as compared to C.

The measured responses of Fig. 10 have been used to validate the model and analysis presented in Section II-B. For that purpose, we have extracted the model parameters for each experimental response using the method applied in [84]. Although there is a direct correspondence between the applied bias and the diode capacitance, parasitics have forced us to consider the diode capacitance, C_s, as a parameter that must be extracted. The results of the extraction are depicted in Table I. The parameter that experiences the most important change with the applied bias is the diode capacitance, as expected. Nevertheless, the conductance also varies somewhat due to the parasitic effects of the diode. As indicated, the change of regime occurs when the applied bias changes from 10 to 11 V, with a diode capacitance variation from 0.50 to

This article has been accepted for inclusion in a future issue of this journal. Content is final as presented, with the exception of pagination.

0.40 pF, although the closest response to critical coupling is the one corresponding to 11-V bias voltage. The circuit responses with extracted parameters are also included in Fig. 10, and the agreement is good. This validates the model of the structure with the presence of the varactor diode.

In the right column of Table I, we include the real part of the impedance at resonance, $R(\omega_0)$, as inferred from expression (14), and the results are coherent with the loss regime, i.e., low-loss regime if $R(\omega_0) < 50\ \Omega$, and high-loss regime if $R(\omega_0) > 50\ \Omega$, indicated in the left column of the table. The value of $R(\omega_0) = 50.38\ \Omega$ for 11 V of applied bias confirms that this response is the closest to the critical coupling (or change of loss regime). We have also evaluated (18) by considering the element values corresponding to the bias voltage of 11 V (except C_s) and the resulting value inferred from (18) is $C_s = 0.40$ pF, i.e., identical to the capacitance where the change of regime occurs, according to Table I (this further confirms the validity of the model and analysis).

According to the hypothesis made at the beginning of this section, it should be expected that, starting from over-coupled mode operation with 100% fat milk, the device should switch to the low-loss regime (under-coupled mode) by increasing the concentration of water (or decreasing the concentration of milk). Moreover, it should be expected that, as the bias voltage increases (forcing the sensor to move progressively away from the critical coupling point), the transition to the low-loss regime (switch-mode) occurs for an increasingly higher concentration of water, thereby providing a mechanism to tune the threshold water concentration (i.e., the one where the sensor switches from the high-loss to the low-loss regime). This has been verified experimentally, as shown in Fig. 11. The figure depicts the frequency responses (magnitude and phase) for different bias voltages and different (small) DI water concentrations. For each bias voltage, the transition from the high-loss to the low-loss regime occurs at the concentration of water where the phase slope at resonance changes from a positive to a negative value (note that the phases are depicted unwrapped in Fig. 11). This transition is very sudden and generates an abrupt phase change at resonance, as Fig. 12 illustrates (such figure depicts the phase of the reflection coefficient at the resonance frequency when pure fat milk fills the capillary).

Fig. 12 indicates the threshold water concentration for each applied voltage. According to these results, it follows that it is possible to tune and identify such a threshold level, and hence it is possible to ensure the purity of fat milk above a certain (predefined) threshold from phase measurements. Note that error bars, corresponding to the standard deviation for each phase point after three measurements, are included in Fig. 12. As can be seen, the standard deviation is small. It should be mentioned that the effects of temperature are not negligible, as discussed later in this article (see Section III-D). However, as far as the temperature is controlled (24 °C in the experiments of Figs. 10–12), the repeatability of the phase measurements is very reasonable.

Sensor versatility, or its capability to be applied to different types of milk (besides fat milk, the case example analyzed and validated before), is an important aspect. According to

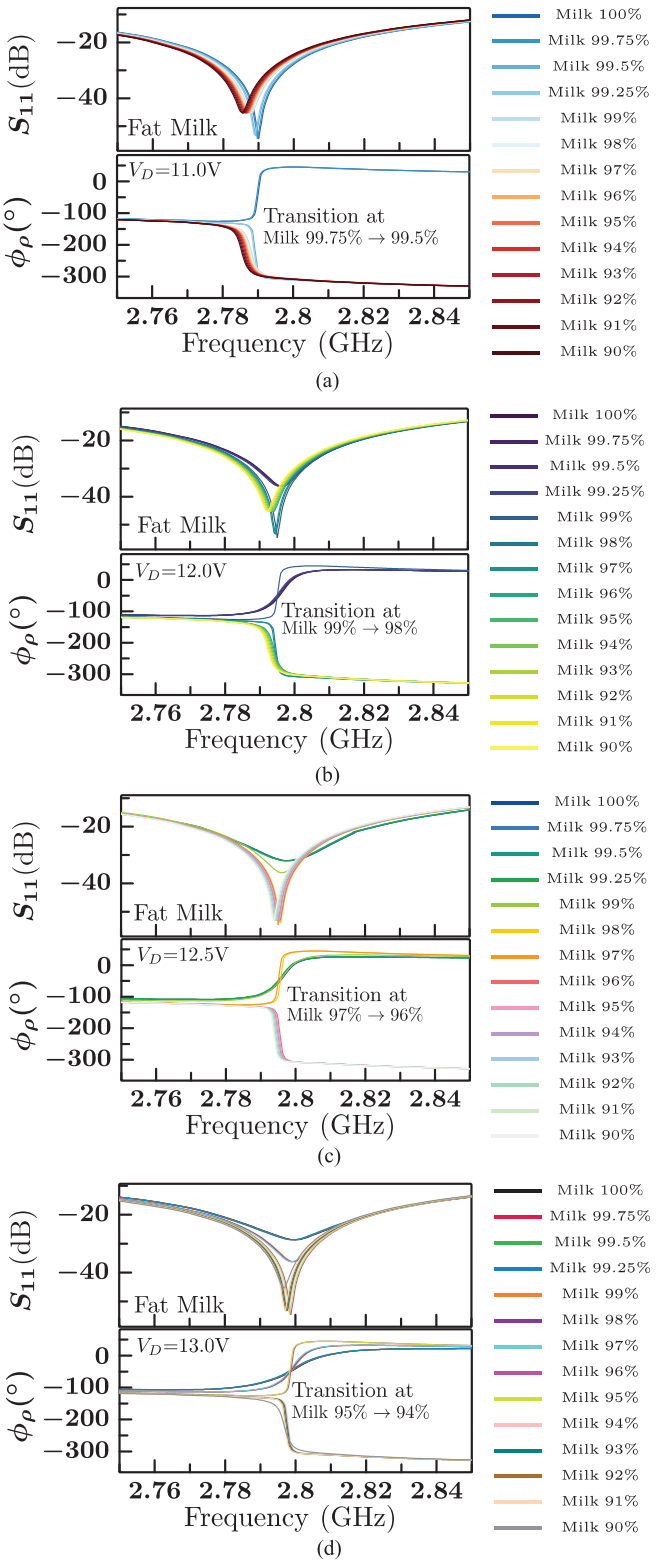


Fig. 11. Measured frequency responses for the fabricated reconfigurable sensor for solutions of fat milk and DI water with different concentrations in the capillary. The bias voltages are: (a) $V_D = 11.0$ V; (b) $V_D = 12.0$ V; (c) $V_D = 12.5$ V; and (d) $V_D = 13.0$ V. The phase is depicted unwrapped. The temperature is 24 °C.

Fig. 1, the dielectric properties of semi-skim and skim milk do not differ so much from those of fat milk. Consequently, it is expected that, by properly tuning the varactor diode, the

This article has been accepted for inclusion in a future issue of this journal. Content is final as presented, with the exception of pagination.

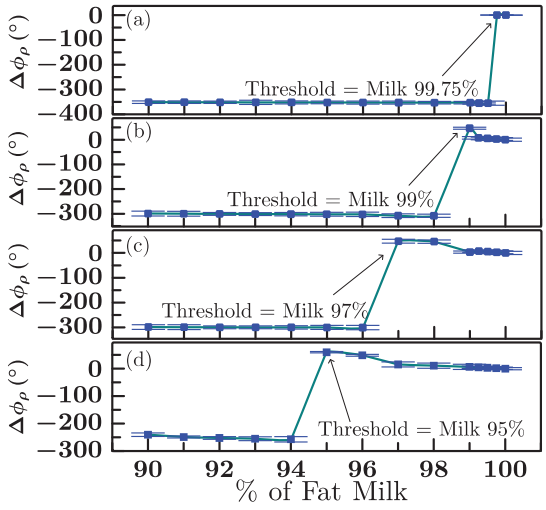


Fig. 12. Measured phase of the reflection coefficient at the resonance frequency when pure fat milk fills the capillary as a function of the fat milk concentration. The bias voltages are: (a) V_D = 11.0 V; (b) V_D = 12.0 V; (c) V_D = 12.5 V; and (d) V_D = 13.0 V. The temperature is 24 °C.

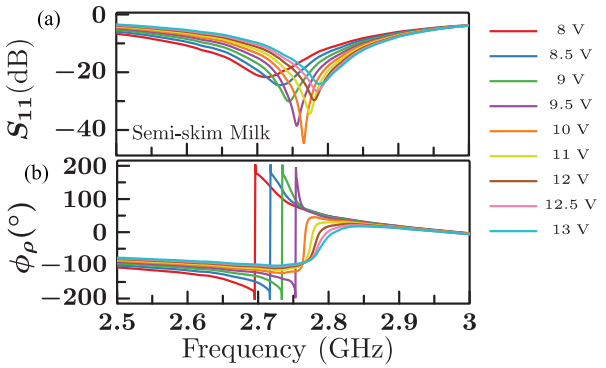


Fig. 13. Measured frequency responses of the fabricated reconfigurable sensor, i.e., magnitude and wrapped phase, for the indicated applied voltages, with the capillary containing 100% pure semi-skim milk in all cases. The measurements have been carried out with the *Keysight 5221A* VNA. The temperature is 24 °C.

threshold water concentration can also be adjusted at will in semi-skim and skim milk (avoiding the need to use a different sensor for each milk type). To validate such sensor versatility, we have repeated the experiments, providing the results depicted in Figs. 10–12 by considering semi-skim and skim milk.

For semi-skim milk, Fig. 13 depicts the measured frequency responses with the capillary full of such milk and different applied voltages. In this case, the transition from the low-loss to the high-loss regime occurs when the applied voltage changes between V_D = 9.5 V and V_D = 10 V. The measured phase and magnitude responses as the water concentration varies and for different applied voltages are not shown, but, from the inferred data, we have obtained the phase of the reflection coefficient at the resonance frequency when pure semi-skim milk fills the capillary as a function of the milk concentration, see Fig. 14. As can be seen, the threshold water concentration can also be precisely controlled with the applied bias (V_D) for semi-skim milk.

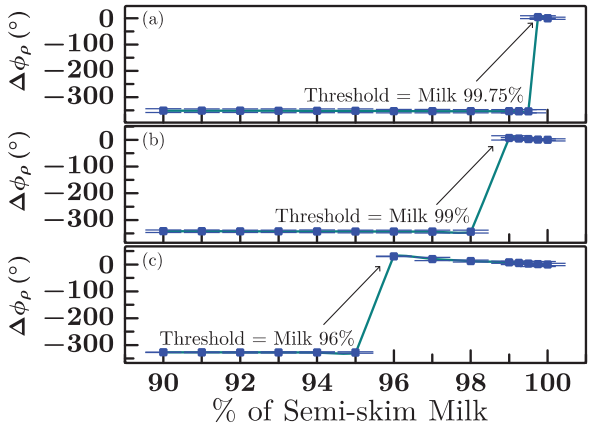


Fig. 14. Measured phase of the reflection coefficient at the resonance frequency when pure semi-skim milk fills the capillary as a function of the semi-skim milk concentration. The bias voltages are: (a) V_D = 10.0 V; (b) V_D = 11.0 V; and (c) V_D = 12 V. The temperature is 24 °C.

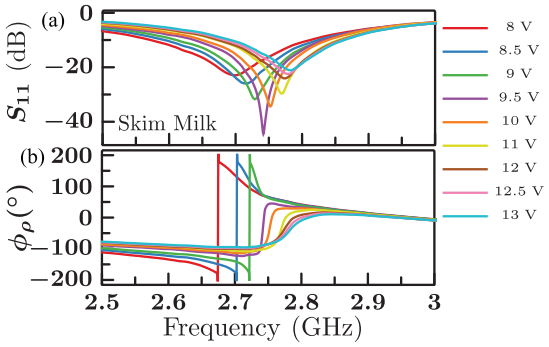


Fig. 15. Measured magnitude and wrapped phase responses of the fabricated sensor, for the indicated applied voltages, with the capillary containing pure skim milk in all cases. The measurements have been carried out with the *Keysight 5221A* VNA. The temperature is 24 °C.

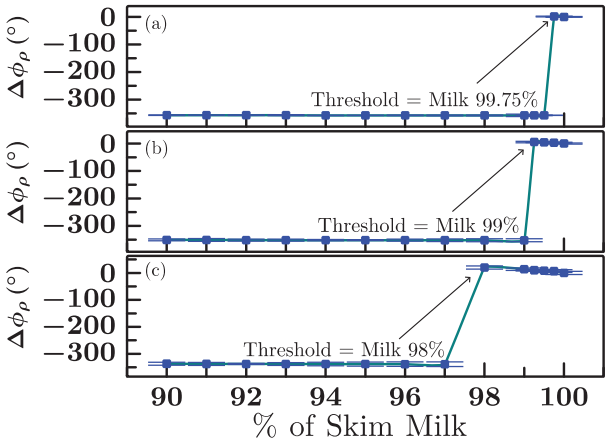


Fig. 16. Measured phase of the reflection coefficient at the resonance frequency when pure skim milk fills the capillary as a function of the skim milk concentration. The bias voltages are: (a) V_D = 9.5 V; (b) V_D = 10.0 V; and (c) V_D = 11 V. The temperature is 24 °C.

Finally, the same experiments carried out with skim milk are depicted in Figs. 15 and 16. With the capillary full of such milk and different applied voltages, the transition from the low-loss to the high-loss regime occurs when the applied voltage changes between V_D = 9.0 V and V_D = 9.5 V (see

This article has been accepted for inclusion in a future issue of this journal. Content is final as presented, with the exception of pagination.

Fig. 15), slightly lower than for semi-skim milk. According to Fig. 16, the threshold water concentration can also be controlled with accuracy for skim milk.

According to Figs. 12, 14, and 16, the standard deviation is much smaller than the phase window between both states (i.e., concentration of milk above or below the threshold). Thus, the error in classification (or the error in determining whether the concentration of water is above or below a predefined threshold) is given by the measured step (as far as the phase repeatability is good on both sides of the threshold, as demonstrated in the indicated figures). The step for milk concentrations smaller than 99% is 1%. Consequently, we will consider that the error in determining if the purity of milk is above or below a certain threshold is 1%, rather than 0.25% (the concentration step in the range between 99% and 100% milk). However, it is shown in Figs. 12, 14, and 16 that for V_D = 11 V, V_D = 10.0 V, and V_D = 9.5 V, respectively, the threshold water concentration is 0.25%, with a sudden change in the phase response in all cases. This concentration value (0.25%) can be assimilated with the sensor resolution, or the minimum water concentration that can be detected, provided the temperature is accurately controlled.

We should mention that, from the unwrapped phase, as depicted in Fig. 11, determining whether the measured sample exhibits a concentration of milk above or below the threshold is very simple. Namely, above the resonance frequency, the unwrapped phase is in the vicinity of 0° for the high-loss regime, whereas for the low-loss regime, the phase is near −360°. Thus, the unwrapped phase measured at a certain frequency, at resonance or above it, suffices for the indicated purpose. However, to obtain the unwrapped phase with the VNA, it is necessary to perform a narrowband measurement (a single-frequency measurement does not suffice) that includes the frequency interval where the significant phase variation around resonance occurs. With the VNA, it does not represent a significant issue (note that such interval is extremely narrow, on account of Fig. 11). Let us also mention that determining the operation regime (high loss or low loss) can also be done from the derivative of the unwrapped phase response, always negative in the low-loss regime, and exhibiting a positive peak around resonance in the high-loss regime.

D. Effects of Temperature

Typically, the complex dielectric constant of liquids exhibits a significant dependence on temperature. Therefore, to gain insight into the effects of temperature, we have carried out measurements at different temperatures. The specific procedure for temperature control was as follows. The samples (different mixtures of milk and water) were prepared in order to have a final volume of 10 mL (though actually, the liquid volume inside the capillary during measurement, with a diameter of 4 mm and a length of 18 cm, was roughly 2.3 mL). Next, such samples were all heated to the desired temperature with the heater mantle and subsequently introduced into the humidity chamber with a stabilized temperature. For measurement of a certain sample, it was extracted from the chamber and injected into the capillary, where the measurements for

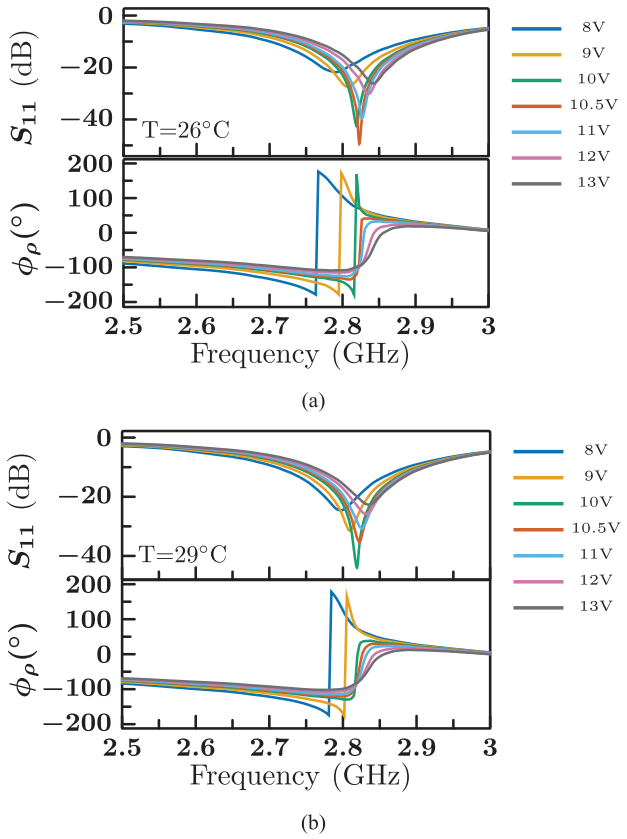


Fig. 17. Measured frequency responses, i.e., magnitude and wrapped phase, of the fabricated reconfigurable sensor for the indicated applied voltages, with the capillary containing 100% pure fat milk in all cases and temperatures of (a) T = 26 °C and (b) T = 29 °C.

different voltages applied to the varactor were carried out. Such measurements are quite fast (less than one minute), and hence a very small temperature variation was expected during measurement. Nevertheless, by using a Peltier device, the temperature can be further (and continuously) controlled and stabilized while contributing to generating a complete standalone fluidic system with temperature control, but this aspect is out of scope in the present article. The complete measurement cycle of all samples took less than 1 h for each type of milk (note that three independent measurements per sample and voltage were done).

Fig. 17 depicts the responses for different voltages when the capillary is filled with pure fat milk measured at T = 26 °C and 29 °C (note that these figures are equivalent to Fig. 10, inferred at 24 °C). According to these results, the higher the temperature, the lower the bias voltage needed to change the loss regime.

For T = 26 °C, we have obtained the frequency responses for different bias voltages and different concentrations of fat milk (equivalent to Fig. 11), and from the obtained results, we have inferred the dependence of the phase at the operating frequency on the concentration of milk; see Fig. 18 (equivalent to Fig. 12). As can be appreciated, for this higher temperature (T = 26°), the voltages necessary to achieve the same threshold concentrations as in Fig. 12 (inferred at T = 24 °C) are smaller. Thus, the effects of temperature are not negligible and demand accurate control of it to properly

This article has been accepted for inclusion in a future issue of this journal. Content is final as presented, with the exception of pagination.

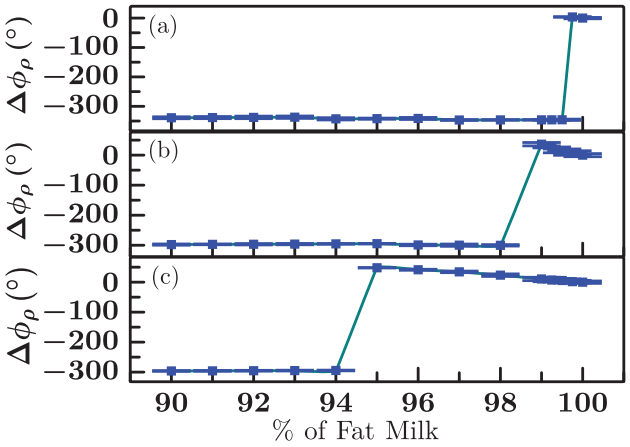


Fig. 18. Measured phase of the reflection coefficient at the resonance frequency when pure fat milk fills the capillary as a function of the fat milk concentration. The bias voltages are: (a) V_D = 10.5 V; (b) V_D = 11.0 V; and (c) V_D = 12.0 V. The temperature is 26 °C.

detect if, for a certain milk under test, its purity is better than a certain threshold. As previously indicated, the step for milk concentrations smaller than 99% is 1%, i.e., the considered error. Nevertheless, such a value is meaningful if the temperature is controlled with accuracy. For 12-V bias, the threshold at 24 °C is 99%, whereas it is 95% at 26 °C, i.e., a variation of 4% with 2 °C change. In addition, for 11 V, the threshold at 24 °C is 99.75%, whereas it is 99% at 26 °C, i.e., a variation of 0.75% for the same change in temperature. Thus, the variation of the temperature does not generate a linear variation in the thresholds. It is thus clear that temperature control is important and necessary to provide good classification estimations (concentration of water below or above the threshold).

E. Uncertainty and Robustness Analysis

To end this section, let us comment on the uncertainty in mixture preparation. The different water/milk mixtures are prepared by using a pipette with a resolution of 0.001 milliliters (mL). In all cases, the total sum of milk and water volume is 10 mL, as indicated before (for example, to prepare a mixture of 99% milk and 1% water, we use 9.9 mL of milk and 0.1 mL of water). To quantify how this resolution in volume (0.001 mL) translates to resolution in the concentration of water in the prepared samples, let us call V_w and V_m the water and milk volumes, respectively, so that $V_m + V_w$ = 10 mL, and let us call ΔV the indicated resolution, i.e., ΔV = 0.001 mL. Indeed, considering the indicated volume resolution, the water and milk volumes are actually $\Delta V_w \pm V$ and $\Delta V_m \pm V$, respectively. Thus, the concentration of water can be expressed as

$$C = \frac{V_w \pm \Delta V}{(V_m \pm \Delta V) + (V_w \pm \Delta V)} = \frac{V_w \pm \Delta V}{V_m + V_w \pm \Delta 2V}. \tag{20}$$

From which it follows that:

$$C = \frac{V_w}{(V_m + V_w)} \cdot \frac{\left(1 \pm \frac{\Delta V}{V_w}\right)}{\left(1 \pm \frac{2\Delta V}{V_m + V_w}\right)}. \tag{21}$$

Let us next calculate the resolution in the concentration of water considering the worst case scenario, i.e., when the volume of water is the lowest one considered, i.e., V_w = 0.025 mL (and hence the volume of milk is V_m = 9.975, so that $V_w + V_m$ = 10 mL, and the concentration of water is 0.25%). Introducing these quantities in (21) gives

$$C = \frac{0.025\left(1 \pm \frac{0.001}{0.025}\right)}{10\left(1 \pm \frac{0.002}{10}\right)} \approx 0.0025\,(1 \pm 0.04)\,. \tag{22}$$

Namely, the relative error in the nominal concentration in the worst case is 4%, which means that the concentration of water in this case (in percentage) is 0.25% ±0.01%. For larger water concentrations, the relative error is smaller, but the absolute error is always 0.01%, as inferred from (21). With the resolution of the considered pipette, the precision in the nominal concentration of water is very good, even for small water concentrations.

The threshold in each set of measurements occurs where matching is achieved for a specific sample. This makes the threshold prone to changes in the sensor characteristics, potentially due to fabrication-related tolerances or to any variation in the varactor diode. Thus, to avoid variations in the threshold level when replicas of the sensor are implemented, the fabrication system must be very robust.

To finalize this section, let us consider an experiment aimed at demonstrating that the switching transition is reproducible and robust around a certain concentration threshold, controlled by the voltage applied to the varactor diode. Thus, additional measurements were performed at a controlled temperature of 24 °C, considering fat milk as a reference. The varactor bias voltage was fixed at 12.5 V [giving a threshold concentration of 97%, according to Fig. 12(c), and a transition region between 96% and 97%]. Samples with milk concentrations ranging from 95% to 98% were prepared at 0.5% intervals. In addition, samples with concentrations of 96.25% and 96.75% were also prepared to provide finer concentration intervals around the transition region. The samples with concentrations from 95% to 96% and from 97% to 98% were measured three times at each concentration. The samples within the transition region (96.25%, 96.5%, and 96.75%) were measured 15 times at each concentration to more thoroughly characterize the variability of the sensor response near the loss-regime transition.

Fig. 19 shows the phase distribution measured at the frequency of operation, whereas Table II summarizes the loss regime occurrence for each sample. As shown in the figure and summarized in the table, milk concentrations below 96% consistently exhibit the low-loss regime, whereas for concentrations above 97% the measured phases are coherent with the high-loss regime. The results are consistent with those shown in Fig. 12(c), where the loss-regime transition occurs within the milk concentration range of 96%–97% at a fixed bias voltage of 12.5 V. Within the transition region, the 96.25% concentration consistently remains in the low-loss regime, while the 96.5% concentration exhibits a mixed response, with 86.67% of the measurements occurring in the low-loss regime and the remaining 13.33% in the high-loss regime. At 96.75%, the response predominantly shifts to the

This article has been accepted for inclusion in a future issue of this journal. Content is final as presented, with the exception of pagination.

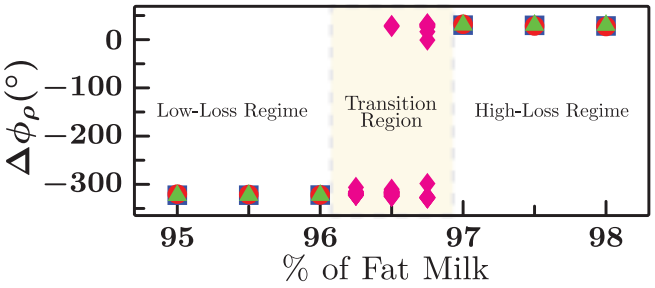


Fig. 19. Statistical analysis of the measured phase of the reflection coefficient at the resonance frequency when pure fat milk fills the capillary for fat milk concentrations in the vicinity of the phase transition (for a bias voltage of V_D = 12.5 V and temperature of 24 °C). A total of 63 measurements, according to the procedure indicated in the text, have been carried out.

TABLE II
STATISTICAL ANALYSIS OF THE RESULTS OF FIG. 19

Milk (%)	No. Meas	Loss Regime Occurrence		Loss Regime Occurrence Percentage		Result
		Low	High	Low (%)	High (%)	
95	3	3	0	100	0	Stable low loss
95.5	3	3	0	100	0	Stable low loss
96	3	3	0	100	0	Stable low loss
96.25	15	15	0	100	0	Stable low loss
96.5	15	13	2	86.67	13.33	Transition
96.75	15	5	10	33.33	66.67	Transition
97	3	0	3	0	100	Stable high loss
97.5	3	0	3	0	100	Stable high loss
98	3	0	3	0	100	Stable high loss

high-loss regime. These results demonstrate the presence of mixed loss-regime behavior within the transition region, point out that the switching transition is reproducible and robust around the concentration threshold, and further confirm that the error in sample classification is better than 1%.

IV. DISCUSSION AND USE OF GAIN/PHASE DETECTOR

Even though low-cost VNAs are commercially available, there may be applications where the price of the VNA penalizes the overall system cost. Thus, in this section we explore and discuss the strategy to replace the VNA with a gain-phase detector. The system is depicted in Fig. 20. Note that, in a real environment, to further reduce system cost, the input signal should be generated by means of a microwave oscillator, e.g., a VCO managed by a microcontroller. However, in this preliminary proof-of-concept prototype, we have chosen to use a signal generator. The system architecture utilizes a broadband quadrature coupler (the details are out of the scope of this article), in charge of injecting the input signal to the sensor and retrieving the reflected signal from it. The isolated and coupled ports are driven to the input ports of the gain-phase detector through circulators (acting as isolators). By this means, any

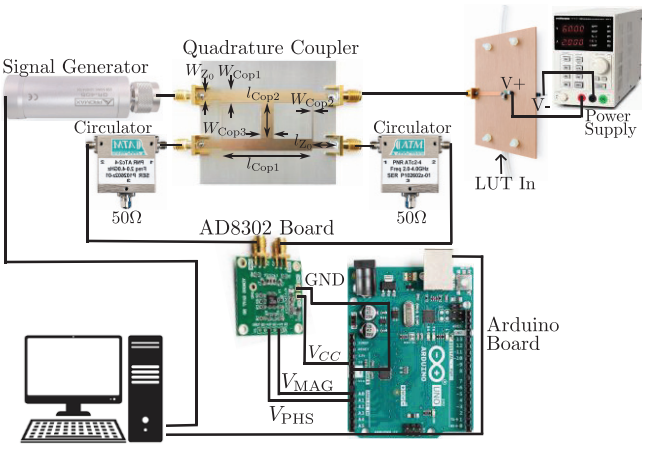


Fig. 20. System architecture using a gain-phase detector (model *Analog Devices AD8302*) managed by a microcontroller (model *Arduino UNO*). The signal generator is the *Promax* model *GR-405*, the DC power supply is the *Tenma* model *72-10505*, and the circulator is the *Advanced Technical Materials (ATM)* model *ATC2-4*. The coupler is implemented in the *Isola I-Tera MT40 (RF/MW)* microwave substrate with dielectric constant ε_r = 3.55, thickness h = 1.524 h = 1.524 mm, and loss tangent tanδ = 0.0022. Dimensions of the coupler (in mm) are: W_{Cop1} = 6, l_{Cop1} = 38, W_{Cop2} = 0.485, l_{Cop2} = 18.55, W_{Cop3} = 5.5, W_{Z0} = 3.36, and l_{Z_0} = 10. The optimum temperature for operation of the phase detector (with smaller phase and magnitude error) is around 25 °C [93], very close to the temperature in the measurement campaigns (24 °C).

reflected signal generated from potential mismatches from the gain-phase detector is absorbed by the 50-Ω loads of the circulators. With this configuration, a voltage proportional to the phase difference between the input ports of the gain-phase detector (designated as V_{PHS} in Fig. 20), in turn related to the phase of the reflection coefficient of the sensing element, is generated. Similarly, the detector generates a voltage (V_{MAG}) related to the magnitude of the reflection coefficient (the details can be found in [60]). Finally, the retrieved data from the detector, managed by the microcontroller, can be visualized or postprocessed using, e.g., a computer. The diode voltage is generated by means of a variable DC power supply in this work, but simpler and cheaper schemes can be envisaged for real application (e.g., a digital-to-analog converter (DAC) managed by the microcontroller).

To validate the system, we have considered only mixtures of fat milk and DI water with concentrations ranging from 100% to 90% of fat milk, with steps of 1% (finer variations of 0.25% were applied between 100% and 99% to capture small changes in the sensor response). The prepared mixtures were introduced into the capillary, integrated with the sensor. For each concentration, three voltage levels were applied to the varactor: V_D = 9 V, V_D = 9.5 V, and V_D = 10 V, whereas the sensor was excited (using the signal generator) with a signal in the frequency range of 2.4–2.6 GHz. Let us mention that the upper frequency limit of operation of the available gain-phase detector (*Analog Devices AD8302*) is 2.7 GHz. For this reason, we have slightly modified the dimensions of the sensor, so that the new resonance frequencies lie in the vicinity of 2.5 GHz. Particularly, we have increased the length of the DB-DGS slot to 60 mm (the other dimensions are kept unaltered). This justifies the indicated frequency range (2.4–2.6 GHz) of the signal generator, different than that of

This article has been accepted for inclusion in a future issue of this journal. Content is final as presented, with the exception of pagination.

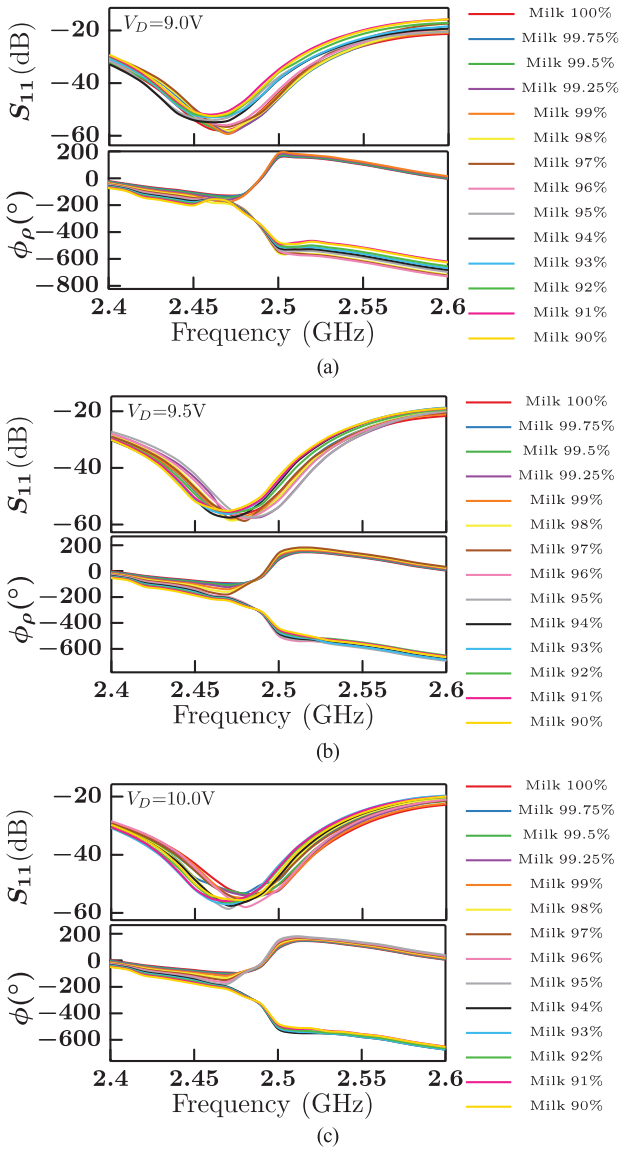


Fig. 21. Measured frequency responses for the reconfigurable sensor for solutions of fat milk and DI water with different concentrations in the capillary, inferred with the system of Fig. 20. The bias voltages are: (a) V_D = 9 V; (b) V_D = 9.5 V; and (c) V_D = 10 V.

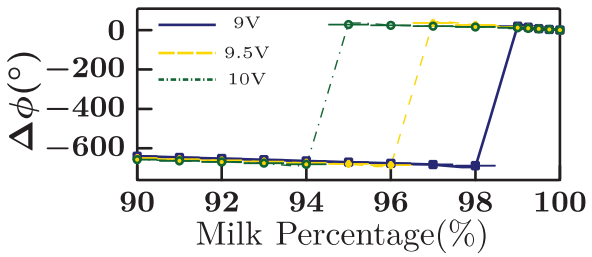


Fig. 22. Measured phase of the reflection coefficient at 2.5 GHz as a function of the fat milk concentration for the indicated bias voltages.

the VNA in Section III (2.7–2.9 GHz). Each measurement was repeated three times to ensure reliability and consistency of the results.

Fig. 21 depicts the phase and magnitude responses for the different indicated applied voltages and for the different concentrations, whereas Fig. 22 depicts the phase measured

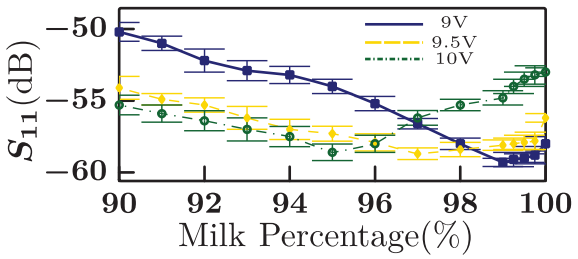


Fig. 23. Measured lowest magnitude of the response as a function of the fat milk concentrations for the indicated applied voltages.

at 2.5 GHz as a function of milk concentration (for the three considered voltages), using as reference the phase when pure fat milk is present in the capillary. Like the case with VNA, the unwrapped phase responses, inferred after postprocessing, exhibit a distinct behavior for the high-loss and low-loss regimes. The threshold concentrations for each applied voltage are clearly visible in Fig. 22, i.e., 99%, 97%, and 95% for V_D = 9 V, V_D = 9.5 V, and V_D = 10 V, respectively. From the phase response of an unknown sample, obtained for a certain applied voltage, we can determine if the concentration of milk is above or below the considered threshold corresponding to that voltage (the operation regime determines this). The distinction between the low-loss and the high-loss regimes is more clearly identified through phase analysis, as compared to magnitude analysis. In particular, the unwrapped phase response provides a more pronounced transition between these regimes compared to the magnitude response, making it a useful parameter for detecting the threshold behavior of the sensor.

However, in this measurement setup, unlike a VNA, which isolates and measures the intrinsic response of the sensor, the measured phase represents the overall system response. This includes additional phase contributions from cables, connectors, and other components in the signal path. Consequently, the measured phase does not accurately reflect the true phase response of the sensor. A similar limitation applies to the magnitude response, where the measured values represent the combined effect of the entire system rather than solely the intrinsic behavior of the sensor. From these observations, it can be concluded that the measured values are influenced by the overall system rather than solely reflecting the intrinsic response of the sensor. Although magnitude-based measurements are less affected by such effects, as discussed earlier, the distinction between the high-loss and the low-loss regime is not clearly appreciable from the magnitude response. The reason is that the magnitude responses are similar, regardless of the specific regime of operation. Nevertheless, the frequency response for the transition between both regimes, corresponding to critical coupling, as discussed, is characterized by the strongest attenuation of the reflected signal at resonance (i.e., the return loss at resonance is a maximum, or the reflection coefficient magnitude is a minimum). This can be appreciated in Fig. 23, which exhibits the lowest value of the magnitude response for various milk percentages measured at V_D = 9 V, V_D = 9.5 V, and V_D = 10 V. It can be seen from the figure that the minimum magnitude exhibits a V-shaped behavior,

This article has been accepted for inclusion in a future issue of this journal. Content is final as presented, with the exception of pagination.

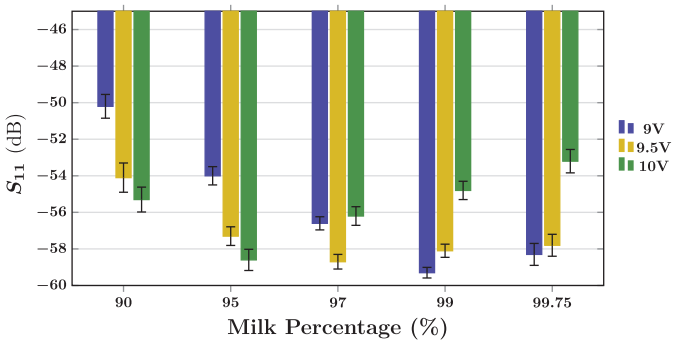


Fig. 24. Measured lowest magnitude of the response for five specific fat milk concentrations and for the indicated applied voltages.

where the minimum value for each voltage corresponds to the threshold milk concentration for that voltage.

To determine whether an unknown mixture is above or below a certain concentration threshold using the magnitude, rather than the phase, the procedure, involving measurements with the system of Fig. 20 at three different voltages, is as follows. First, the magnitude response at the voltage corresponding to the considered threshold must be recorded. If the minimum value coincides with the minimum of Fig. 23 for that voltage, it means that the concentration coincides with the threshold. By contrast, if the minimum magnitude in the measured response is above the minimum of Fig. 23 for that voltage, two alternative milk concentrations are possible, i.e., below or above the threshold, by virtue of the V-shaped curves in Fig. 23. To distinguish between these two possibilities, the idea is to obtain the minimum magnitude for an applied voltage below and above that of the initial measurements (giving the threshold). A smaller value of the measured minimum magnitude for the lower voltage, as compared to the one of the higher voltages, indicates that the milk concentration of the unknown sample is above the threshold. By contrast, if the concentration is below the threshold, it is expected that the measured minimum value of the response is higher for the lower applied voltage.

To validate the approach, we have depicted in Fig. 24 the minimum magnitude value for five different milk concentrations and the three considered voltages applied to the varactor (9, 9.5, and 10 V). Inspection of this figure clearly confirms that the method reported in the previous paragraph is valid. For example, let us assume that the unknown milk concentration is 90% and that the threshold is 97% (occurring when V_D = 9.5 V). The measured minima at V_D = 9 V for 90% concentration is larger than the one measured when V_D = 10 V, and, therefore, the concentration is below the threshold. If, by contrast, the concentration of the unknown sample is, e.g., 99% or 99. 75%, the opposite trend occurs, meaning that the concentrations are above the threshold.

Using this approach, postprocessing is not required, as the analysis only relies on identifying the minimum magnitude in the measured response. Furthermore, this method is less affected by variations introduced by cables and other system components, since it focuses on relative trends rather than absolute values. However, the proposed method has some limitations. First, the measurement must be performed over a certain (narrowband) frequency range, as single-frequency measurements are not sufficient to determine the minimum value of the magnitude response, occurring at resonance (indeed, narrowband measurements are also required by using a VNA, as discussed in the preceding section). Second, measurements must be conducted at three bias voltage levels, since the classification relies on observing the trend of magnitude variation across different voltages. To achieve finer resolution in threshold detection, additional bias voltage levels may be required. Finally, prior knowledge of the bias voltage corresponding to the threshold condition for a given mixture is required. This information is essential as a reference for interpreting variations in the magnitude response. Consequently, phase measurements with unwrapped phase analysis must be conducted beforehand to accurately determine the threshold points.

Although the proposed method requires measurements over a certain frequency range and for several bias voltages, and it depends on prior knowledge of threshold conditions, it offers a practical measurement approach without the need for a VNA. Nevertheless, it should be mentioned that the accuracy of the method is not as good as that of the one with a VNA (the error bars depicted in Figs. 22 and 23, obtained after three independent measurements, reveal that the dispersion is larger as compared to the phase measurements of Figs. 12, 14, 16, and 18).

V. Comparative Analysis

Rather than being applied to volume fraction determination in binary mixtures, the reported sensor is devoted to detecting the presence of water in milk above a certain controllable threshold. It acts as a threshold-based classification device rather than as a quantitative concentration measurement sensor. The device is an unconventional sensing element, based on switch-mode operation (and hence extremely nonlinear), which means that the main used sensing metric, i.e., the maximum sensitivity (or the average sensitivity), does not apply in any comparison with other sensors. The two main distinctive features of the presented switch-mode sensor over its competitors are: 1) the capability to detect very small percentages of water in milk (with 0.25% resolution, provided the temperature is accurately controlled), regardless of the type of milk (fat, semi-skim, and skim), demonstrated by measuring with a VNA and 2) the possibility to control (through electronic tuning) the threshold water concentration, important to determine if the purity level of the considered milk satisfies a certain requirement (given by such threshold).

Concerning the first aspect, the achieved percentage of detection for small concentrations of water is 0.25% and can be assimilated to the resolution of the sensor (although the considered error in classifying a certain sample above or below the threshold concentration is 1%, as justified before). Table III presents other sensors devoted to volume fraction determination in binary mixtures, including devices focused on water–milk [9], [11] like the present one. In some cases, the achieved resolution is excellent, e.g., in the device presented in [76]. However, it should be mentioned that the dielectric properties of the components of the binary solutions in such

This article has been accepted for inclusion in a future issue of this journal. Content is final as presented, with the exception of pagination.

TABLE III
COMPARISON OF LIQUID SENSORS FOR VOLUME FRACTION DETERMINATION IN BINARY MIXTURES

Ref.	Principle	Sensing size (λ_g^2)	Reconfigurability /Contactless	Resolution (%)
[9]	Frequency	0.603	No/Yes	20
[11]	Frequency	0.452	No/No	25
[94]	Frequency	0.0049	No/No	5
[12]	Frequency	0.022	No/No	10
[95]	Frequency	0.0079	No/Yes	10
[96]	Magnitude	0.0075	No/No	5
[97]	Magnitude	0.047	No/No	5
[66]	Phase	0.0002	No/No	2
[68]	Phase	0.0016	No/No	0.5
[76]	Phase	0.0104	No/No	0.07
[44]	Magnitude	0.0485	No/No	1
[62]	Phase	0.003	No/No	10
[98]	Frequency	0.026	No/No	10
[99]	Frequency	0.32	No/No	10
[100]	Frequency	0.051	No/No	10
[20]	Frequency	0.021	No/Yes	0.005
[101]	Frequency	0.0019	No/Yes	0.1
[102]	Frequency	0.2112	No/No	10
[103]	Frequency	0.0412	No/Yes	20
[104]	Phase	0.003	No/No	10
[105]	Frequency	0.0523	No/No	20
[106]	Frequency	0.0365	No/No	3
[107]	Frequency	0.0439	No/No	15
[108]	Frequency	0.13	No/No	1
[109]	Freq/Mag.	---	No/No	1
[82a]	Phase	0.0017	No/No	1
[82b]	Phase	0.0019	No/No	2.5
[84]	Phase	0.0078	No/Yes	0.25
T.W.*	**Phase**	**0.0593**	**Yes/Yes**	**0.25**

*Corresponds to the VNA-based system.

sensors are significantly different (and thus the detection of small quantities of solute is simpler), as compared to water and milk, with very similar dielectric constants. In addition, the reported sensor is contactless, contrary to most sensors reported in Table III, where the LUT is in direct contact with the sensing element.

Concerning reconfigurability (tunability), it has two important benefits. One concerns the control of the threshold water concentration, as indicated. The second advantageous aspect is versatility, namely, the possibility of using the switch-mode sensor for determining product purity in different types of milks, as has been demonstrated with the VNA-based version of the device. Other reconfigurable sensors based on different tuning principles (mechanical [83], JFETs [72], and varactor diodes [85]) have been recently reported but not applied to liquid sensing.

In summary, the high resolution, reconfigurability, and versatility are unique features of the reported switch-mode sensor, not found simultaneously in its competitors. Moreover, the sensor is extremely simple and small (the areas of the sensing region expressed in terms of the squared wavelength are also included in Table III). We left for future work the application of the sensor to milks (fat, skim, and semi-skim) of different producers, since the final goal of this research activity is the implementation of a prototype that can be used in a real environment, e.g., in bottling plants, where cleaning with water makes the use of systems to guarantee product (milk) purity. The sensor can also potentially be applied to detect adulterated milk with water. By tuning the bias voltage of the diode, the threshold concentration can be adjusted, as demonstrated. However, if a certain type of milk is analyzed for the first time, a calibration to know the dependence of the threshold concentration on the applied bias is needed.

VI. CONCLUSION

In conclusion, we have proposed and experimentally validated a reflective-mode reconfigurable switch-mode phase-variation sensor by applying it to detect small concentrations of DI water in different types of milk (fat, semi-skim, and skim). The relevant and novel aspect of the proposed sensor concerns the possibility of detecting the presence of a controllable concentration of water, designated as a threshold, which determines the level of purity. This is possible by virtue of the sudden change of operating regime (from the high-loss to the low-loss regime) that takes place at such a threshold. This generates an abrupt change in the phase response, the measurable quantity, so that the sensor operates as a binary (or switchable) device. The key aspect to achieve such binary behavior is to design the sensor to operate close to the critical coupling condition (or change of regime) when the capillary used to drive the LUT to the sensing region, a DB-DGS resonator, contains pure milk. Since the proximity to such critical coupling can be adjusted by the capacitance of the varactor diode, it follows that by tuning such a varactor diode with an external voltage, we can adjust at will the threshold water concentration. With a VNA as the measuring device, sensor functionality has been demonstrated with the above-indicated types of milk (of a specific brand at a temperature of 24 °C). In all cases, the threshold water concentration has been adjusted by the tuning voltage. It has been shown that the threshold water concentration can be set to small values (0.25%). Nevertheless, the demonstrated classification error is 1% since this is the water (or milk) concentration step in the different measurements for milk concentrations in the range 90%–99% (the concentration step in the range 99%–100% has been 0.25%). Moreover, it has been demonstrated the functionality of the sensor not only by using a VNA as a measurement device, but also by considering a gain-phase detector and the associated electronics. In this latter case, it has been concluded that using the magnitude response is preferred over the phase, and a method to determine if the milk concentration of a certain unknown sample is above or below the threshold has been proposed and validated. The accuracy of this method is not comparable to the one with VNA (it exhibits a coarser threshold detection) based on the phase response, but the use of a gain-phase detector provides a low-cost alternative that can be useful in certain situations where the use of a VNA is prohibitive. We left for future work aspects such as how to minimize the presence of air in the capillary when the milk under analysis is derived from the bottling pipes in an industrial environment, or the possibility of detecting other adulterant agents in milk. Concerning the latter aspect, since the dielectric properties of such adulterants are

This article has been accepted for inclusion in a future issue of this journal. Content is final as presented, with the exception of pagination.

different than those of water, we would need to know them in advance for properly measuring their concentrations. The issue of selectivity for detecting different species of adulterant agents is a challenge, and it will probably require a machine-learning assisted approach, left also for future work.

REFERENCES

[1] O. A. Talkhan, "Milk adulteration: Some chemical adulterants of milk," *Egyptian J. Chem. Environ. Health*, vol. 1, no. 1, pp. 694–703, Nov. 2015.

[2] A. K. Yadav, M. Gattupalli, K. Dashora, and V. Kumar, "Key milk adulterants in India and their detection techniques: A review," *Food Anal. Methods*, vol. 16, no. 3, pp. 499–514, Mar. 2023.

[3] P. J. Ahranjani, K. Dehghan, Z. Esfandiari, and P. J. Ahranjani, "A systematic review of spectroscopic techniques for detecting milk adulteration," *Crit. Rev. Anal. Chem.*, vol. 56, no. 4, pp. 1–32, May 2026.

[4] T. Azad and S. Ahmed, "Common milk adulteration and their detection techniques," *Int. J. Food Contamination*, vol. 3, no. 1, Dec. 2016, Art. no. 22.

[5] A. Poonia, A. Jha, R. Sharma, H. B. Singh, A. K. Rai, and N. Sharma, "Detection of adulteration in milk: A review," *Int. J. Dairy Technol.*, vol. 70, no. 1, pp. 23–42, 2017.

[6] X. Zhu, W. Guo, and Z. Liang, "Determination of the fat content in cow's milk based on dielectric properties," *Food Bioprocess Technol.*, vol. 8, no. 7, pp. 1485–1494, Jul. 2015.

[7] X. Zhu, Q. Liu, and W. Guo, "Dielectric properties of raw milk as influenced by frequency, salts, and salt contents," *J. Food Process Eng.*, vol. 41, no. 7, Nov. 2018, Art. no. e12885.

[8] S. N. Abdullah, K. Y. You, N. Hisham Khamis, and C. Y. Chong, "Modelling the dielectric properties of cow's raw milk under vat pasteurization," *Prog. Electromagn. Res. M*, vol. 84, pp. 157–166, 2019.

[9] S. Jain, N. K. Tiwari, and M. Jaleel Akhtar, "CSIWC RFsensor for micro-fluidicnon-contactquality assessment of milk," *Int. J. RF Microw. Comput.-Aided Eng.*, vol. 32, no. 2, Feb. 2022, Art. no. e22962.

[10] Q. Liang, Y. Liu, H. Zhang, J. Che, Y. Xia, and S. Li, "Non-destructive detection of water adulteration level in fresh milk based on combination of dielectric spectrum technology and machine learning method," *J. Food Composition Anal.*, vol. 136, Dec. 2024, Art. no. 106807.

[11] S. Aiswarya, L. Meenu, K. A. U. Menon, M. Donelli, and S. K. Menon, "A novel microstrip sensor based on closed loop antenna for adulteration detection of liquid samples," *IEEE Sensors J.*, vol. 24, no. 2, pp. 1405–1414, Jan. 2024.

[12] A. Ebrahimi, W. Withayachumnankul, S. Al-Sarawi, and D. Abbott, "High-sensitivity metamaterial-inspired sensor for microfluidic dielectric characterization," *IEEE Sensors J.*, vol. 14, no. 5, pp. 1345–1351, May 2014.

[13] M. Schueler, C. Mandel, M. Puentes, and R. Jakoby, "Metamaterial inspired microwave sensors," *IEEE Microw. Mag.*, vol. 13, no. 2, pp. 57–68, Mar. 2012.

[14] M. S. Boybay and O. M. Ramahi, "Material characterization using complementary split-ring resonators," *IEEE Trans. Instrum. Meas.*, vol. 61, no. 11, pp. 3039–3046, Nov. 2012.

[15] C.-S. Lee and C.-L. Yang, "Complementary split-ring resonators for measuring dielectric constants and loss tangents," *IEEE Microw. Wireless Compon. Lett.*, vol. 24, no. 8, pp. 563–565, Aug. 2014.

[16] C.-L. Yang, C.-S. Lee, K.-W. Chen, and K.-Z. Chen, "Noncontact measurement of complex permittivity and thickness by using planar resonators," *IEEE Trans. Microw. Theory Techn.*, vol. 64, no. 1, pp. 247–257, Jan. 2016.

[17] L. Su, J. Mata-Contreras, P. Vélez, A. Fernández-Prieto, and F. Martín, "Analytical method to estimate the complex permittivity of oil samples," *Sensors*, vol. 18, no. 4, p. 984, Mar. 2018.

[18] M. Abdolrazzaghi, M. H. Zarifi, W. Pedrycz, and M. Daneshmand, "Robust ultra-high resolution microwave planar sensor using fuzzy neural network approach," *IEEE Sensors J.*, vol. 17, no. 2, pp. 323–332, Jan. 2017.

[19] M. H. Zarifi et al., "A microwave ring resonator sensor for early detection of breaches in pipeline coatings," *IEEE Trans. Ind. Electron.*, vol. 65, no. 2, pp. 1626–1635, Feb. 2018.

[20] M. Abdolrazzaghi, M. Daneshmand, and A. K. Iyer, "Strongly enhanced sensitivity in planar microwave sensors based on metamaterial coupling," *IEEE Trans. Microw. Theory Techn.*, vol. 66, no. 4, pp. 1843–1855, Apr. 2018.

[21] H. Lobato-Morales, J. H. Choi, H. Lee, and J. L. Medina-Monroy, "Compact dielectric-permittivity sensors of liquid samples based on substrate-integrated-waveguide with negative-order-resonance," *IEEE Sensors J.*, vol. 19, no. 19, pp. 8694–8699, Oct. 2019.

[22] A. K. Jha, N. Delmonte, A. Lamecki, M. Mrozowski, and M. Bozzi, "Design of microwave-based angular displacement sensor," *IEEE Microw. Wireless Compon. Lett.*, vol. 29, no. 4, pp. 306–308, Apr. 2019.

[23] A. Ebrahimi, J. Scott, and K. Ghorbani, "Ultrahigh-sensitivity microwave sensor for microfluidic complex permittivity measurement," *IEEE Trans. Microw. Theory Techn.*, vol. 67, no. 10, pp. 4269–4277, Oct. 2019.

[24] M. Saadat-Safa, V. Nayyeri, A. Ghadimi, M. Soleimani, and O. M. Ramahi, "A pixelated microwave near-field sensor for precise characterization of dielectric materials," *Sci. Rep.*, vol. 9, no. 1, Sep. 2019, Art. no. 13310.

[25] M. Abdolrazzaghi and M. Daneshmand, "Exploiting sensitivity enhancement in micro-wave planar sensors using intermodulation products with phase noise analysis," *IEEE Trans. Circuits Syst. I, Reg. Papers*, vol. 67, no. 12, pp. 4382–4395, Dec. 2020.

[26] A. Ebrahimi, J. Scott, and K. Ghorbani, "Microwave reflective biosensor for glucose level detection in aqueous solutions," *Sens. Actuators A, Phys.*, vol. 301, Jan. 2020, Art. no. 111662.

[27] A. Ebrahimi, J. Scott, and K. Ghorbani, "Dual-mode resonator for simultaneous permittivity and thickness measurement of dielectrics," *IEEE Sensors J.*, vol. 20, no. 1, pp. 185–192, Jan. 2020.

[28] H. Abdelwahab, A. Ebrahimi, F. J. Tovar-Lopez, G. Beziuk, and K. Ghorbani, "Extremely sensitive microwave microfluidic dielectric sensor using a transmission line loaded with shunt LC resonators," *Sensors*, vol. 21, no. 20, p. 6811, Oct. 2021.

[29] J. Muñoz-Enano, J. Martel, P. Vélez, F. Medina, L. Su, and F. Martín, "Parametric analysis of the edge capacitance of uniform slots and application to frequency-variation permittivity sensors," *Appl. Sci.*, vol. 11, no. 15, p. 7000, Jul. 2021.

[30] N. Kazemi, M. Abdolrazzaghi, and P. Musilek, "Comparative analysis of machine learning techniques for temperature compensation in microwave sensors," *IEEE Trans. Microw. Theory Techn.*, vol. 69, no. 9, pp. 4223–4236, Sep. 2021.

[31] Z. Mehrjoo, A. Ebrahimi, and K. Ghorbani, "Microwave resonance-based reflective mode displacement sensor with wide dynamic range," *IEEE Trans. Instrum. Meas.*, vol. 71, pp. 1–9, 2022.

[32] J. Muñoz-Enano, P. Vélez, M. Gil, and F. Martín, "Frequency-variation sensors for permittivity measurements based on dumbbell-shaped defect ground structures (DB-DGS): Analytical method and sensitivity analysis," *IEEE Sensors J.*, vol. 22, no. 10, pp. 9378–9386, May 2022.

[33] S. Mohammadi, K. K. Adhikari, M. C. Jain, and M. H. Zarifi, "High-resolution, sensitivity-enhanced active resonator sensor using substrate-embedded channel for characterizing low-concentration liquid mixtures," *IEEE Trans. Microw. Theory Techn.*, vol. 70, no. 1, pp. 576–586, Jan. 2022.

[34] M. Moradpour and M. H. Zarifi, "High-resolution PEDOT: PSS-based planar microwave resonator sensor," *IEEE Sensors J.*, vol. 23, no. 18, pp. 21216–21225, Sep. 2023.

[35] M. A. Rafi, F. Niknahad, B. D. Wiltshire, A. Salim, and M. H. Zarifi, "Dynamically tunable planar microwave resonator sensor using liquid metal alloy," *IEEE Trans. Microw. Theory Techn.*, vol. 72, no. 7, pp. 4103–4113, Jul. 2024.

[36] P. Vélez et al., "Single-frequency amplitude-modulation sensor for dielectric characterization of solids and microfluidics," *IEEE Sensors J.*, vol. 21, no. 10, pp. 12189–12201, May 2021.

[37] A. Ebrahimi, G. Beziuk, and K. Ghorbani, "Amplitude variation microwave sensors for high-sensitivity detection of solid and microfluidic dielectrics," *IEEE Trans. Microw. Theory Techn.*, vol. 72, no. 11, pp. 6460–6472, Nov. 2024.

[38] Z. R. Omam, V. Nayyeri, S.-H. Javid-Hosseini, and O. M. Ramahi, "Simple and high-sensitivity dielectric constant measurement using a high-directivity microstrip coupled-line directional coupler," *IEEE Trans. Microw. Theory Techn.*, vol. 70, no. 8, pp. 3933–3942, Aug. 2022.

[39] A. Ebrahimi and K. Ghorbani, "High-sensitivity detection of solid and liquid dielectrics using a branch line coupler sensor," *IEEE Trans. Microw. Theory Techn.*, vol. 71, no. 12, pp. 5233–5245, Dec. 2023.

[40] C. Damm, M. Schüßler, M. Puentes, H. Maune, M. Maasch, and R. Jakoby, "Artificial transmission lines for high sensitive microwave sensors," in *Proc. IEEE Sensors*, Christchurch, New Zealand, Oct. 2009, pp. 755–758.

This article has been accepted for inclusion in a future issue of this journal. Content is final as presented, with the exception of pagination.

[41] F. Ferrández-Pastor, J. García-Chamizo, and M. Nieto-Hidalgo, "Electromagnetic differential measuring method: Application in microstrip sensors developing," *Sensors*, vol. 17, no. 7, p. 1650, Jul. 2017.

[42] J. Muñoz-Enano, P. Vélez, M. G. Barba, and F. Martín, "An analytical method to implement high-sensitivity transmission line differential sensors for dielectric constant measurements," *IEEE Sensors J.*, vol. 20, no. 1, pp. 178–184, Jan. 2020.

[43] M. Gil, P. Vélez, F. Aznar-Ballesta, J. Muñoz-Enano, and F. Martín, "Differential sensor based on electroinductive wave transmission lines for dielectric constant measurements and defect detection," *IEEE Trans. Antennas Propag.*, vol. 68, no. 3, pp. 1876–1886, Mar. 2020.

[44] J. Muñoz-Enano, P. Vélez, M. G. Barba, J. Mata-Contreras, and F. Martín, "Differential-mode to common-mode conversion detector based on rat-race hybrid couplers: Analysis and application to differential sensors and comparators," *IEEE Trans. Microw. Theory Techn.*, vol. 68, no. 4, pp. 1312–1325, Apr. 2020.

[45] J. Coromina et al., "Capacitively-loaded slow-wave transmission lines for sensitivity improvement in phase-variation permittivity sensors," in *Proc. 50th Eur. Microw. Conf. (EuMC)*, Jan. 2021, pp. 491–494.

[46] A. Ebrahimi et al., "Highly sensitive phase-variation dielectric constant sensor based on a capacitively-loaded slow-wave transmission line," *IEEE Trans. Circuits Syst. I, Reg. Papers*, vol. 68, no. 7, pp. 2787–2799, Jul. 2021.

[47] L. Su, J. Muñoz-Enano, P. Vélez, P. Casacuberta, M. Gil, and F. Martín, "Phase-variation microwave sensor for permittivity measurements based on a high-impedance half-wavelength transmission line," *IEEE Sensors J.*, vol. 21, no. 9, pp. 10647–10656, May 2021.

[48] A. Ebrahimi, J. Muñoz-Enano, P. Vélez, J. Scott, K. Ghorbani, and F. Martín, "Phase variation microfluidic permittivity sensor using a dispersive transmission line," in *Proc. IEEE Sensors*, Dallas, TX, USA, Oct. 2022, pp. 1–4.

[49] A. K. Jha, A. Lamecki, M. Mrozowski, and M. Bozzi, "A highly sensitive planar microwave sensor for detecting direction and angle of rotation," *IEEE Trans. Microw. Theory Techn.*, vol. 68, no. 4, pp. 1598–1609, Apr. 2020.

[50] J. Muñoz-Enano, P. Vélez, L. Su, M. Gil, P. Casacuberta, and F. Martín, "On the sensitivity of reflective-mode phase-variation sensors based on open-ended stepped-impedance transmission lines: Theoretical analysis and experimental validation," *IEEE Trans. Microw. Theory Techn.*, vol. 69, no. 1, pp. 308–324, Jan. 2021.

[51] L. Su, J. Muñoz-Enano, P. Velez, P. C. Orta, M. Gil, and F. Martin, "Highly sensitive phase variation sensors based on step-impedance coplanar waveguide (CPW) transmission lines," *IEEE Sensors J.*, vol. 21, no. 3, pp. 2864–2872, Feb. 2021.

[52] P. Casacuberta, J. Muñoz-Enano, P. Vélez, L. Su, M. Gil, and F. Martín, "Highly sensitive reflective-mode defect detectors and dielectric constant sensors based on open-ended stepped-impedance transmission lines," *Sensors*, vol. 20, no. 21, p. 6236, Oct. 2020.

[53] L. Su, J. Muñoz-Enano, P. Vélez, M. Gil-Barba, P. Casacuberta, and F. Martin, "Highly sensitive reflective-mode phase-variation permittivity sensor based on a coplanar waveguide terminated with an open complementary split ring resonator (OCSRR)," *IEEE Access*, vol. 9, pp. 27928–27944, 2021.

[54] P. Casacuberta et al., "Circuit analysis of a coplanar waveguide (CPW) terminated with a step-impedance resonator (SIR) for highly sensitive one-port permittivity sensing," *IEEE Access*, vol. 10, pp. 62597–62612, 2022.

[55] Z. Mehrjoo, A. Ebrahimi, and K. Ghorbani, "Phase variation reflective-mode displacement sensor using a CPW loaded with dumbbell-shaped resonator," in *Proc. IEEE Asia Pacific Microw. Conf. (APMC)*, Nov. 2021, pp. 467–469.

[56] A. K. Horestani, Z. Shaterian, and F. Martín, "Rotation sensor based on the cross-polarized excitation of split ring resonators (SRRs)," *IEEE Sensors J.*, vol. 20, no. 17, pp. 9706–9714, Sep. 2020.

[57] J. Muñoz-Enano, P. Vélez, L. Su, M. Gil-Barba, and F. Martín, "A reflective-mode phase-variation displacement sensor," *IEEE Access*, vol. 8, pp. 189565–189575, 2020.

[58] P. Casacuberta, P. Vélez, J. Muñoz-Enano, L. Su, and F. Martín, "Highly sensitive reflective-mode phase-variation permittivity sensors using coupled line sections," *IEEE Trans. Microw. Theory Techn.*, vol. 71, no. 7, pp. 2970–2984, Jul. 2023.

[59] P. Casacuberta, P. Vélez, J. Muñoz-Enano, L. Su, M. Gil, and F. Martín, "Reflective-mode phase-variation permittivity sensors based on coupled resonators,", "Reflective-mode phase-variation permittivity sensors based on coupled resonators," in *Proc. IEEE Sensors*, Dallas, TX, USA, Oct. 2022, pp. 1–4.

[60] M. Elgeziry, F. Paredes, P. Vélez, F. Costa, S. Genovesi, and F. Martín, "A method to retrieve the output variables in reflective-mode phase-variation sensors," in *Proc. 52nd Eur. Microw. Conf. (EuMC)*, Milan, Italy, Sep. 2022, pp. 516–519.

[61] P. Vélez et al., "Portable reflective-mode phase-variation microwave sensor based on a rat-race coupler pair and Gain/Phase detector for dielectric characterization," *IEEE Sensors J.*, vol. 23, no. 6, pp. 5745–5756, Mar. 2023.

[62] L. Su, P. Casacuberta, P. Vélez, J. Muñoz-Enano, M. Gil, and F. Martín, "Reflective-mode submersible microwave sensor," in *Proc. IEEE Sensors*, Dallas, TX, USA, Oct. 2022, pp. 1–4.

[63] P. Vélez, X. Canalias, J. Muñoz-Enano, P. Casacuberta, L. Su, and F. Martín, "Effects of losses on the sensitivity of reflective-mode phase-variation liquid sensors," *IEEE Trans. Microw. Theory Techn.*, vol. 72, no. 2, pp. 903–918, Feb. 2024.

[64] P. Casacuberta, P. Vélez, J. Muñoz-Enano, L. Su, and F. Martín, "Losses assisted sensitivity enhancement in reflective-mode phase-variation permittivity sensors based on weakly coupled distributed resonators," *IEEE Sensors Lett.*, vol. 7, no. 8, pp. 1–4, Aug. 2023.

[65] P. Casacuberta, P. Vélez, J. Muñoz-Enano, L. Su, and F. Martín, "Highly sensitive coplanar waveguide (CPW) reflective-mode phase-variation permittivity sensors based on weakly coupled step-impedance resonators (SIRs)," *IEEE Trans. Microw. Theory Techn.*, vol. 72, no. 3, pp. 1739–1753, Mar. 2024.

[66] L. Su, P. Vélez, P. Casacuberta, J. Muñoz-Enano, M. Gil-Barba, and F. Martín, "Reflective-mode phase-variation submersible sensor for liquid characterization," *IEEE Trans. Instrum. Meas.*, vol. 72, 2023, Art. no. 6009412.

[67] Z. Mehrjoo, A. Ebrahimi, and K. Ghorbani, "Analytical design of phase variation-based dielectric constant sensors," in *Proc. 53rd Eur. Microw. Conf. (EuMC)*, Berlin, Germany, Sep. 2023, pp. 729–732.

[68] J. Muñoz-Enano, P. Vélez, P. Casacuberta, L. Su, and F. Martín, "Reflective-mode phase-variation permittivity sensor based on a step-impedance microstrip line terminated with a slot resonator for solid and liquid characterization," *IEEE Trans. Microw. Theory Techn.*, vol. 72, no. 4, pp. 2519–2533, Apr. 2024.

[69] A. Karami-Horestani, F. Paredes, and F. Martín, "Phase-variation microwave displacement sensor with good linearity and application to breath rate monitoring," *IEEE Sensors J.*, vol. 23, no. 19, pp. 22486–22495, Oct. 2023.

[70] Z. Mehrjoo, A. Ebrahimi, G. Beziuk, F. Martín, and K. Ghorbani, "Microwave rotation sensor based on reflection phase in transmission lines terminated with lumped resonators," *IEEE Sensors J.*, vol. 23, no. 7, pp. 6571–6580, Apr. 2023.

[71] M. Elgeziry, F. Costa, P. Vélez, F. Paredes, F. Martín, and S. Genovesi, "Toward a low-cost portable reader for reflective-mode microwave sensors," *IEEE Trans. Instrum. Meas.*, vol. 73, pp. 1–9, 2024.

[72] P. Casacuberta, P. Vélez, L. Su, X. Canalias, and F. Martín, "Highly sensitive lossy tunable permittivity sensor," *IEEE Microw. Wireless Technol. Lett.*, vol. 34, no. 6, pp. 687–690, Jun. 2024.

[73] P. Casacuberta, P. Vélez, J. Muñoz-Enano, L. Su, and F. Martín, "Highly sensitive phase-variation microwave sensor for measuring the thickness of dielectric films on metals with micrometer-scale resolution," in *Proc. IEEE/MTT-S Int. Microw. Symp. (IMS)*, San Diego, CA, USA, Jun. 2023, pp. 959–962.

[74] A. Karami-Horestani et al., "Reflective-mode phase-variation sensors based on a movable step impedance resonator (SIR) and application to micrometer-scale motion sensing," *IEEE Trans. Microw. Theory Techn.*, vol. 73, no. 1, pp. 592–605, Jan. 2025.

[75] X. Canalias, P. Vélez, P. Casacuberta, L. Su, and F. Martín, "Transmission-mode phase-variation planar microwave sensor based on a step-impedance shunt stub for high sensitivity defect detection, dielectric constant, and proximity measurements," *IEEE Trans. Microw. Theory Techn.*, vol. 73, no. 2, pp. 1017–1028, Feb. 2025.

[76] P. Casacuberta, P. Vélez, L. Su, X. Canalias, and F. Martín, "Sensitive microfluidic sensor with weakly coupled dumbbell defect-ground-structure resonators for volume fraction determination in liquid mixtures," *IEEE Microw. Wireless Technol. Lett.*, vol. 34, no. 12, pp. 1411–1414, Dec. 2024.

[77] P. Casacuberta et al., "Sensitivity optimization in single-frequency planar microwave sensors for solid and liquid characterization and microfluidics," *IEEE Trans. Microw. Theory Techn.*, vol. 73, no. 3, pp. 1581–1609, Mar. 2025.

[78] X. Canalias, P. Casacuberta, P. Vélez, L. Su, and F. Martín, "Highly sensitive transmission-mode phase-variation permittivity sensor based on resonance and antiresonance," *IEEE Trans. Microw. Theory Techn.*, vol. 73, no. 3, pp. 1619–1631, Mar. 2025.

This article has been accepted for inclusion in a future issue of this journal. Content is final as presented, with the exception of pagination.

[79] P. Casacuberta, P. Vélez, L. Su, X. Canalias, and F. Martín, "Engineering with loss to enhance sensitivity in microwave sensors," *IEEE Microw. Mag.*, vol. 26, no. 5, pp. 52–66, May 2025.

[80] N. Kurniawati, P. Vélez, P. Casacuberta, L. Su, X. Canalias, and F. Martín, "Highly sensitive phase-variation microwave sensor operating in transmission based on an open split ring resonator (OSRR)," *IEEE Sensors J.*, vol. 24, no. 24, pp. 40749–40763, Dec. 2024.

[81] J. Borràs-Sarsa, P. Casacuberta, P. Vélez, L. Su, X. Canalias, and F. Martín, "Microstrip configurations of reflective-mode phase-variation permittivity sensors based on weakly coupled step impedance resonators (SIR): An analysis to the light of circuit duality," *IEEE Access*, vol. 13, pp. 85838–85856, 2025.

[82] N. Kurniawati et al., "A versatile reflective-mode phase-variation microwave sensor based on a dumbbell defect-ground-structure (DB-DGS) resonator for solid and liquid characterization," *IEEE Sensors J.*, vol. 25, no. 16, pp. 30676–30691, Aug. 2025.

[83] P. Casacuberta, P. Vélez, L. Su, X. Canalias, N. Kurniawati, and F. Martín, "Mechanically reconfigurable reflective-mode phase-variation sensors: A strategy for sensitivity optimization and control," *IEEE Trans. Microw. Theory Techn.*, vol. 74, no. 3, pp. 2573–2586, Mar. 2026.

[84] N. Kurniawati, P. Vélez, P. Casacuberta, X. Canalias, L. Su, and F. Martín, "Contactless microwave sensor for quality assessment of liquid products," *IEEE Trans. Microw. Theory Techn.*, vol. 74, no. 4, pp. 3677–3688, Apr. 2026.

[85] X. Canalias, P. Vélez, P. Casacuberta, N. Kurniawati, and F. Martín, "Highly sensitive and tunable reflective-mode phase-variation microwave sensor using varactor diode: Application to vibration detection," *IEEE Trans. Microw. Theory Techn.*, vol. 74, no. 5, pp. 4474–4490, May 2026.

[86] W. Shahzad, W. Hu, Q. Ali, A. R. Barket, and G. Shah, "Varactor-based tunable sensor for dielectric measurements of solid and liquid materials," *J. Sensor Actuator Netw.*, vol. 13, no. 1, p. 8, Jan. 2024.

[87] N. Kurniawati, P. Vélez, P. Casacuberta, X. Canalias, G. Sisó, and F. Martín, "Sensitive detection of water in milk using microwaves," in *Proc. IEEE Appl. Sens. Conf. (APSCON)*, Delhi, India, Jul. 2026, pp. 1–4.

[88] R. M. Foster, "A reactance theorem," *Bell Syst. Tech. J.*, vol. 3, no. 2, pp. 259–267, Apr. 1924.

[89] D. M. Pozar, *Microwave Engineering*, 4th ed., Hoboken, NJ, USA: Wiley, 2011.

[90] Z. Wei et al., "A high-sensitivity microfluidic sensor based on a substrate integrated waveguide re-entrant cavity for complex permittivity measurement of liquids," *Sensors*, vol. 18, no. 11, p. 4005, Nov. 2018.

[91] M. Abdolrazzaghi, M. H. Zarifi, and M. Daneshmand, "Sensitivity enhancement of split ring resonator based liquid sensors," in *Proc. IEEE Sensors*, Orlando, FL, USA, Oct. 2016, pp. 1–3.

[92] N. Sharafadinzadeh, M. Abdolrazzaghi, and M. Daneshmand, "Investigation on planar microwave sensors with enhanced sensitivity from microfluidic integration," *Sens. Actuators A, Phys.*, vol. 301, Jan. 2020, Art. no. 111752.

[93] *AD8302: LF-2.7 GHz RF/IF Gain and Phase Detector, Analog Devices*, Wilmington, MA, USA, Sep. 2006.

[94] T. Chretiennot, D. Dubuc, and K. Grenier, "A microwave and microfluidic planar resonator for efficient and accurate complex permittivity characterization of aqueous solutions," *IEEE Trans. Microw. Theory Techn.*, vol. 61, no. 2, pp. 972–978, Feb. 2013.

[95] E. L. Chuma, Y. Iano, G. Fontgalland, and L. L. B. Roger, "Microwave sensor for liquid dielectric characterization based on metamaterial complementary split ring resonator," *IEEE Sensors J.*, vol. 18, no. 24, pp. 9978–9983, Dec. 2018.

[96] P. Vélez, K. Grenier, J. Mata-Contreras, D. Dubuc, and F. Martín, "Highly-sensitive microwave sensors based on open complementary split ring resonators (OCSRRs) for dielectric characterization and solute concentration measurement in liquids," *IEEE Access*, vol. 6, pp. 48324–48338, 2018.

[97] P. Vélez, J. Muñoz-Enano, M. Gil, J. Mata-Contreras, and F. Martín, "Differential microfluidic sensors based on dumbbell-shaped defect ground structures in microstrip technology: Analysis, optimization, and applications," *Sensors*, vol. 19, no. 14, p. 3189, Jul. 2019.

[98] W. Withayachumnankul, K. Jaruwongrungsee, A. Tuantranont, C. Fumeaux, and D. Abbott, "Metamaterial-based microfluidic sensor for dielectric characterization," *Sens. Actuators A, Phys.*, vol. 189, pp. 233–237, Jan. 2013.

[99] A. Salim and S. Lim, "Complementary split-ring resonator-loaded microfluidic ethanol chemical sensor," *Sensors*, vol. 16, no. 11, p. 1802, Oct. 2016.

[100] P. Vélez, L. Su, K. Grenier, J. Mata-Contreras, D. Dubuc, and F. Martín, "Microwave microfluidic sensor based on a microstrip splitter/combiner configuration and split ring resonators (SRRs) for dielectric characterization of liquids," *IEEE Sensors J.*, vol. 17, no. 20, pp. 6589–6598, Oct. 2017.

[101] B. D. Wiltshire and M. H. Zarifi, "3-D printing microfluidic channels with embedded planar microwave resonators for RFID and liquid detection," *IEEE Microw. Wireless Compon. Lett.*, vol. 29, no. 1, pp. 65–67, Jan. 2019.

[102] X. Zhang, C. Ruan, T. U. Haq, and K. Chen, "High-sensitivity microwave sensor for liquid characterization using a complementary circular spiral resonator," *Sensors*, vol. 19, no. 4, p. 787, Feb. 2019.

[103] J. Kilpijärvi, N. Halonen, J. Juuti, and J. Hannu, "Microfluidic microwave sensor for detecting saline in biological range," *Sensors*, vol. 19, no. 4, p. 819, Feb. 2019.

[104] W.-J. Wu, W.-S. Zhao, and W. Wang, "A novel microwave sensor based on modified rat-race coupler for extracting real permittivity and concentration of binary aqueous solution," *IEEE Sensors J.*, vol. 24, no. 9, pp. 14213–14228, May 2024.

[105] S. Kiani, P. Rezaei, and M. Navaei, "Dual-sensing and dual-frequency microwave SRR sensor for liquid samples permittivity detection," *Measurement*, vol. 160, Aug. 2020, Art. no. 107805.

[106] M. Navaei, P. Rezaei, and S. Kiani, "A symmetric bar chart-shape microwave sensor with high q -factor for permittivity determination of fluidics," *Int. J. Microw. Wireless Technol.*, vol. 15, no. 8, pp. 1334–1342, Oct. 2023.

[107] M. Navaei, P. Rezaei, and S. Kiani, "Measurement of low-loss aqueous solutions permittivity with high detection accuracy by a contact and free-label resonance microwave sensor," *Int. J. Commun. Syst.*, vol. 36, no. 5, pp. 1–12, Mar. 2023.

[108] X. Song, G. A. E. Vandenbosch, and S. Yan, "An enhanced microwave differential microfluidic sensing system for detecting small variation of dielectric properties," *IEEE Sensors J.*, vol. 25, no. 6, pp. 9608–9617, Mar. 2025.

[109] S. Seyyedmasoumian, M. Chavoshi, D. Schreurs, B. Nauwelaers, and T. Markovic, "Microwave resonator-based interferometric sensing setup for detection of aqueous solutions," *IEEE Trans. Microw. Theory Techn.*, vol. 74, no. 2, pp. 1634–1649, Feb. 2026.



Nazmia Kurniawati (Graduate Student Member, IEEE) was born in Tangerang, Indonesia, in 1991. She received the bachelor's degree in electrical engineering from the Institut Sains dan Teknologi Nasional, Jakarta, Indonesia, in 2014, and the master's degree in electrical engineering from the Institut Teknologi Sepuluh Nopember, Surabaya, Indonesia, in 2019, with a focus on telecommunications and multimedia studies. She is currently pursuing the Ph.D. degree in electrical engineering at the Universitat Autònoma de Barcelona, Barcelona, Spain, with a focus on the development of planar microwave sensors for the characterization of solid and liquid materials.

This article has been accepted for inclusion in a future issue of this journal. Content is final as presented, with the exception of pagination.



Paris Vélez (Senior Member, IEEE) was born in Barcelona, Spain, in 1982. He received the telecommunications engineering degree, the electronics engineering degree, and the Ph.D. degree in electronics engineering from the Universitat Autònoma de Barcelona (UAB), Barcelona, Spain, in 2008, 2010, and 2014, respectively. His Ph.D. thesis concerned common-mode suppression differential microwave circuits based on metamaterial concepts and semi-lumped resonators.

During the Ph.D., he was awarded a pre-doctoral teaching and research fellowship by Spanish Government from 2011 to 2014. From 2015 to 2017, he was involved in subjects related to metamaterial sensors for fluidics detection and characterization at LAAS-CNRS through a TECNIOSpring Fellowship co-founded by the Marie Curie Program. From 2018 to 2021, he focused his research on the design of high-performance RF/microwave sensors for different applications (structural health and liquid quality control in industrial production) through a Juan de la Cierva Fellowship. His current research interests include the miniaturization of passive RF/microwave circuits and the optimization of microwave sensors through a Ram Ãn y Cajal (2023) Fellowship.

Dr. Vélez is a reviewer of IEEE TRANSACTIONS ON MICROWAVE THEORY AND TECHNIQUES and other journals.



Pau Casacuberta (Member, IEEE) was born in Sabadell, Barcelona, Spain, in 1997. He received the bachelor's degree in electronic telecommunications engineering and computer engineering from the Universitat Autònoma de Barcelona (UAB), Barcelona, in 2020, the master's degree in telecommunications engineering in 2022, and the Ph.D. degree from UAB in December 2025.

He received the Collaboration Fellowship from Spanish Government in 2019 for developing his bachelor's thesis in highly sensitive microwave sensors based on stepped impedance structures. Furthermore, he has been recently intensively working in the elaboration of his Ph.D., focused on the development of microwave sensors for the characterization of the composition of multicomponent liquid substances, with a research grant from the FPU Program of Spanish Ministry of Universities.



Xavier Canalias (Graduate Student Member, IEEE) was born in Sabadell, Barcelona, Spain, in 1999. He received the bachelor's degree in electronic telecommunications engineering and the master's degree in telecommunications engineering from the Universitat Autònoma de Barcelona (UAB), Barcelona, in 2021 and 2023, respectively. He is currently doing the Ph.D. thesis, which is focused on the development of planar microwave sensors implemented by means of semi-lumped and distributed components for the characterization of solids and liquids.



Gerard Sisó was born in Barcelona, Spain, in 1981. He received the B.Sc. degree in industrial engineering (electronics speciality) from the Universitat Politècnica de Catalunya, Barcelona, in 2004 and the M.Sc. and Ph.D. degrees in electronics engineering from the Universitat Autònoma de Barcelona (UAB), Barcelona, in 2006 and 2010, respectively.

He is currently working on topics related to RF/microwave sensors. He acts as a Research Promoter and the Laboratory Manager of GEMMA/CIMITEC, UAB.



Ferran Martín (Fellow, IEEE) was born in Barakaldo, Vizcaya, Spain, in 1965. He received the B.S. degree in physics from the Universitat Autònoma de Barcelona (UAB), Barcelona, Spain, in 1988, and the Ph.D. degree in physics from UAB in 1992.

From 1994 to 2006, he was an Associate Professor of electronics at the Departament d'Enginyeria Electrònica, UAB, and since 2007, he has been a Full Professor of electronics. Throughout his career, he has been very active in research fields as diverse as metamaterials and artificial transmission lines, microwave circuits and filters, antennas, chipless RFID, and planar microwave sensors (his main research topic at present). He is the Head (and Founder) of the Microwave Engineering, Metamaterials and Antennas Group (GEMMA Group), UAB, and the Director (and Founder) of CIMITEC, a research and technology transfer Center ascribed to the Departament d'Enginyeria Electrònica, UAB. He has authored and co-authored over 700 technical conference, letter, journal articles, and book chapters, he is the co-author of the book on Metamaterials titled *Metamaterials with Negative Parameters: Theory, Design and Microwave Applications* (John Wiley & Sons Inc.), the author of the book *Artificial Transmission Lines for RF and Microwave Applications* (John Wiley & Sons Inc.), and the co-author of the book *Time-Domain Signature Barcodes for Chipless-RFID and Sensing Applications* (Springer) and *Planar Microwave Sensors* (Wiley/IEEE Press). He has generated 24 Ph.D. students, has filed several patents on metamaterials, chipless-RFID, and sensors, and has headed dozens of development contracts and collaborative projects with companies.

Prof. Martín is a member of the IEEE Microwave Theory and Techniques Society (IEEE MTT-S). He Martín is a Fellow of IET. He is a reviewer of IEEE TRANSACTIONS ON MICROWAVE THEORY AND TECHNIQUES and IEEE MICROWAVE AND WIRELESS COMPONENTS LETTERS, among many other journals. He serves as a member of the Editorial Board for IEEE TRANSACTIONS ON MICROWAVE THEORY AND TECHNIQUES, IET MICROWAVES, ANTENNAS AND PROPAGATION, and *Sensors*. He is also a member of the Technical Program Committee of European Microwave Conference (EuMC) and a member of the Scientific Advisory Board of the International Congress on Advanced Electromagnetic Materials in Microwaves and Optics (Metamaterials). Among his distinctions, he has received the 2006 Duran Farell Prize for Technological Research, he holds the Parc de Recerca UAB−−Santander Technology Transfer Chair, and he was a recipient of four ICREA ACADEMIA Awards (calls 2008, 2013, 2018, and 2024). He has organized several international events related to metamaterials, chipless-RFID, and sensors, including Workshops at the IEEE International Microwave Symposium (in 2005 and 2007) and European Microwave Conference (in 2009, 2015, 2017, 2018, and 2024), and the Fifth International Congress on Advanced Electromagnetic Materials in Microwaves and Optics (Metamaterials 2011), where he acted as the Chair of the Local Organizing Committee. He has acted as a Guest Editor of seven Special Issues on Metamaterials and Sensors in various international journals. He is a Co-Editor of the book *Balanced Microwave Filters* (Wiley/IEEE Press) and *Coupled Structures for Microwave Sensing* (Springer).